# 4.17 The Chemical Composition of Subducting Sediments

**T Plank**, Lamont-Doherty Earth Observatory of Columbia University, Palisades, NY, USA





## 4.17.1 Introduction

Sediments on the seafloor are records of erosion of the continents and productivity of marine life (see Li and Schoonmaker, 2003; Sageman and Lyons, 2003; Veizer and MacKenzie, 2003; and references therein). Sediments are also input to the world's subduction zones, supplying water and chemical components to arc volcanoes and contaminants to the deeper mantle. This chapter considers how continental, biological, and seawater components mix to create the diversity of chemical compositions recorded in bulk sediments that subduct. Because of the subduction focus, this treatment does not include all marine sediments, notably excluding those on the continental shelves and most of the Atlantic Ocean. Moreover, the goal here is the opposite of that for paleoclimate studies, which aim to recover the highest resolution chemical records. Here, chemical variations are integrated and averaged over large sections of the seafloor to provide estimates of regionally significant bulk input fluxes to trenches. Plank and Langmuir (1998) provided a comprehensive review of the geochemical composition of subducting sediments, estimates for ~25 trenches, and a global average (global subducting sediment (GLOSS)). This chapter updates that effort, including a new assessment of trace elements for which a wealth of inductively coupled plasma mass spectrometry (ICP-MS) data now exists (Nb, Ta, U, Th, and Pb), revised bulk estimates for almost all trenches, and a new global average (GLOSS-II). Notably, new elements (Li, Be, and B) and new trenches (New Zealand and Chile) are included in GLOSS-II.

## 4.17.2 Approach

The subduction problem requires bulk concentration data for a large number of sedimentary samples, in complete sections near deep-sea trenches. It should be obvious that this exercise is completely dependent on the international ocean drilling programs and the samples and data collected by hundreds of seagoing scientists. **Figure 1** provides a map of the near-trench drill sites exploited here for both assessing geochemical variability (**Section 4.17.3**) and arriving at useful trench averages (Electronic **Appendix A** and **Table 1**) and a global average (**Section 4.17.4** and **Table 2**). While large multielement datasets exist at high resolution for some sedimentary intervals, these are usually aimed at specific climate problems and so are of less use to regional and global scale problems. Other approaches attempt to isolate certain terrigenous or biogenic fractions with chemical separations. These datasets are useful for process studies but of less utility in obtaining bulk compositions. Instead, a useful approach has been to sample primary lithologies in a given core (nominally one sample per 1–10 m downcore), analyze thoroughly (the full suite of major

 http://dx.doi.org/10.1016/B978-0-08-095975-7.00319-3 

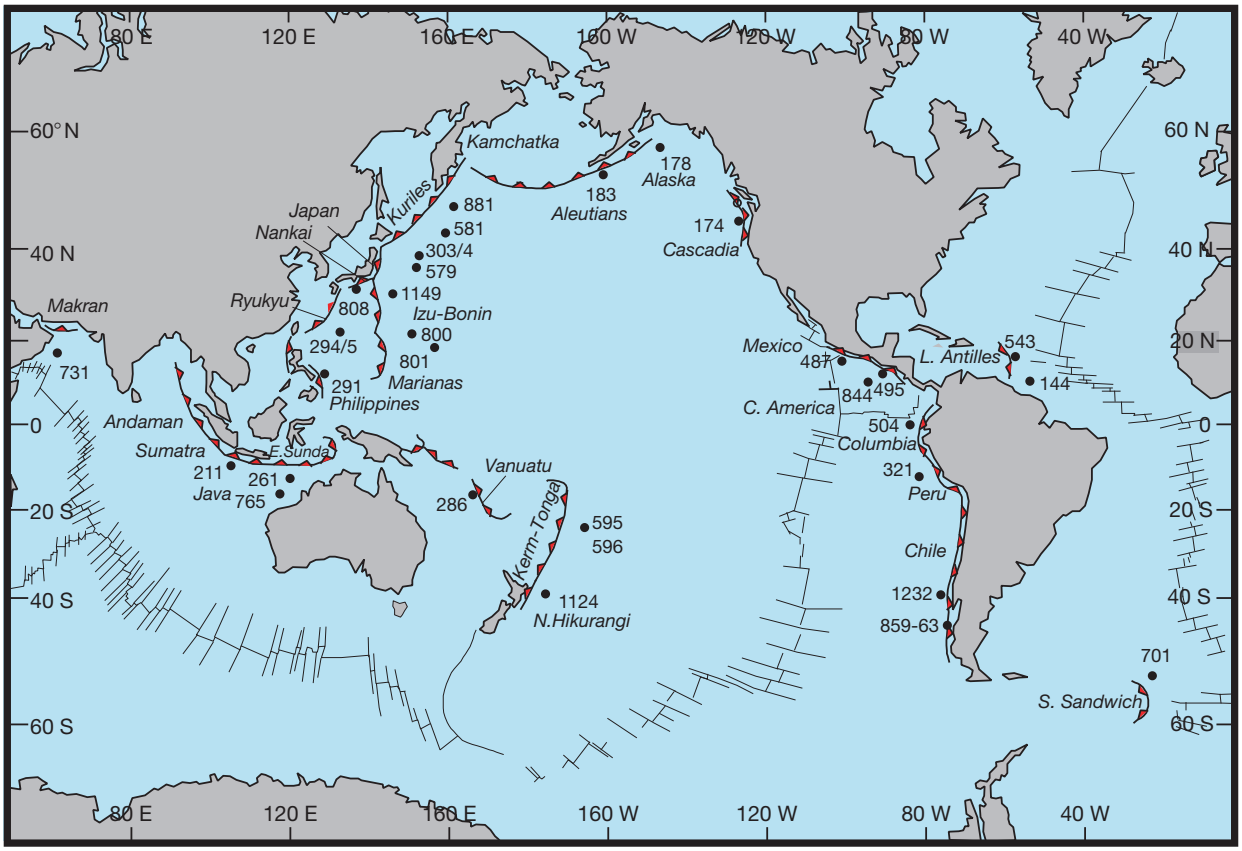


**Figure 1** Map of the world with mid-ocean ridges, convergent margins, and reference DSDP and ODP drill sites used to estimate sediment flux and composition subducting at deep sea trenches.

element, trace element, and isotopic analyses of interest to whole earth problems), and then integrate with continuous lithological descriptions, downhole logging data, and regional seismic stratigraphy. Such an approach can provide bulk compositions within 10% uncertainty (Plank et al., 2007). Since Plank and Langmuir (1998), there have been several studies developing new bulk compositions for specific trenches (notably the Lesser Antilles: Carpentier et al., 2008, 2009; and Izu-Bonin: Chauvel et al., 2009; Plank et al., 2007; Scudder et al., 2009) and new isotope and elemental systematics (Li: Bouman et al., 2004; Chan et al., 2006; and Hf: Chauvel et al., 2008; Vervoort et al., 2011) and a large effort to create a database of marine sediment geochemistry (SedDB: www.seddb.org). In 1998, high-quality ICP-MS data were just coming on the scene but now routinely provide Li, Be, Nb, Ta, U, Th, and Pb concentration data, which were otherwise of variable quality and low in quantity in the original compilation. The current effort focuses on these analytes.

## 4.17.3 Geochemical Systematics in Seafloor Sediments

The geochemical behavior of many solid earth tracers in marine sediments was outlined in Plank and Langmuir (1998). Those findings are summarized here (**Sections** 4.17.3.1–4.17.3.4), and the reader is referred to that work for further details. The perspective that guided that discussion, and this one, is that marine sediments can be treated to first order as mixtures of terrigenous detritus, biogenic phases (calcium carbonate, opal, and apatite), and authigenic phases (metalliferous clays, high in Fe and Mn). Thus, major elements, which aid in the identification of these phases, are essential to understanding trace element and isotopic variation. In the absence of major element data, sedimentological descriptions routinely conducted shipboard, such as smear slide analyses, become useful geochemical information. Sedimentation rate is also an important parameter governing the concentration of some elements in authigenic or biogenic phases.

The words 'pelagic' and 'terrigenous' are common throughout the literature, even though they are not always useful in describing chemical variations. Sediments rich in continental detritus are described here as terrigenous, whether they are found proximally to the continentals (i.e., turbidites) or distally (i.e., pelagic sediments rich in eolian dust). The latter are referred to as terrigenous clays (following the discussion in Vervoort et al., 2011) and can be identified by the lack of Mn or Fe enrichments that are typical of hydrogenetic clays. The term 'pelagic' is generally avoided here because it can include anything from siliceous or carbonate oozes to terrigenous or metalliferous clays, which are all chemically distinct.

#### 4.17.3.1 Alkali Elements (K, Rb, and Cs) and High Field Strength Elements (Nb, Ta, Ti, Zr, and Hf)

The alkali and high field strength elements covary strongly with each other and aluminum, and generally preserve ratios typical of upper continental crust (UCC) or average shales. Thus, to first order, these elements are strongly linked to the detrital phases and the extent of dilution by biogenic phases. Second-order effects on the alkalis include the extent of weathering of the continental source and authigenic clay formation in the ocean. Nb and Nb/Ta variations are discussed further below in the context of new data (Section 4.17.3.9).

#### 4.17.3.2 Sr and Ba

Sr and Ba are strongly linked to biogenic phases (i.e., Sr in biogenic carbonate) and biological productivity (i.e., barite precipitation). Sr varies from 1500 to 2000 ppm in Cenozoic carbonate oozes to 150–200 ppm in average shales. The sediments most enriched in Ba (in wt% quantities) are proximal hydrothermal sediments (which contain precipitated barite) and sediments deposited beneath regions of high biological productivity (where barite precipitates in association with organic matter and siliceous plankton).

#### 4.17.3.3 The Rare Earth Elements and Th

The rare earth elements (REE) and Th are richest in sediments that contain abundant fish debris apatite and Fe–Mn oxides that have accumulated at low sedimentation rates. While the REE pattern of all marine sediments is generally similar to that of the average continental crust, some develop Ce anomalies, which may be negative in hydrothermal and phosphate-rich sediments or positive in Mn-rich sediments. Th variations are discussed further below in the context of new data (Section 4.17.3.11).

#### 4.17.3.4 Uranium

Uranium is notably enriched in sediments that contain organic carbon, which promotes authigenic precipitation of reduced U species. Abundances vary from a few ppm in continental detritus to very low concentrations in biogenic carbonates and opal (<1 ppm) to much higher concentrations in black shales (>10 ppm). U variations are discussed further below in the context of new data (Section 4.17.3.12).

#### 4.17.3.5 New Considerations

Since 1998, new ICP-MS data on marine sediments have provided further insight into some of these element systematics (U, Th, and Nb) and enable new assessments of others (Li, Be, B, and Pb). The behavior of these elements in marine sediments is discussed below, making particular use of ICP-MS data collected using the same methods and standard calibrations (Chan et al., 2006; Plank et al., 2002, 2007; Prytulak et al., 2006; Vervoort et al., 2011; data from all of these studies are reported relative to the standard values in Kelley et al., 2003, with updated values for Li as outlined in Chan et al., 2006). Certain drilled units make useful end-members (e.g., DSDP 174 Cascadia turbidites, ODP 1149 Izu terrigenous clays, and DSDP 294 Ryukyu hydrogenous clays), and these are highlighted in the figures and discussion. Data sources are generally given in figure captions (Figures 2–6). Sedimentary groups (terrigenous turbidites, terrigenous clays, biogenic oozes, hydrogenetic clays, and hydrothermal sediments) generally follow those groupings in Vervoort et al. (2011). Specific reference is made to the UCC average of Rudnick and Gao (see Chapter 4.1) and the post-Archean Australian shale (PAAS) of Taylor and McLennan (1985). A common theme in the discussion is the strength of the detrital signal, and so most elements are compared to $K_2O$, which, like $Al_2O_3$, is primarily detrital in origin (Plank and Langmuir, 1998) but has the added advantage that it is routinely measured by the oceanic drilling programs by natural gamma logging of drilled holes. Some element ratios in marine sediments are so similar to UCC estimates ($Be/K_2O$ and Nb/Ta) that they, in turn, may be used to refine estimates for the average UCC.

#### 4.17.3.6 Lithium and Lithium Isotopes

Lithium is an alkali element and so, to first order, behaves like the other elements in the alkali group (K, Rb, and Cs), varying largely as a function of the detrital, or clay mineral, content of marine sediments. All of these elements show strong correlations with each other and with Al due to dilution by other phases (biogenic silica, biogenic carbonate, detrital quartz, and Fe–Mn–P hydrogenous components). Li varies from 70 to 100 ppm in some clay-rich sediments to less than 2 ppm in biogenic carbonates (Bouman et al., 2004; Chan et al., 2006; Vervoort et al., 2011). Li and $K_2O$ correlate strongly within many sedimentary units, notably hemipelagic sediments dominated by mixtures of biosiliceous material and detrital clays. Several examples are shown in Figure 2(a), where dilution maintains a nearly constant $Li/K_2O$ ratio that is similar to that of average shales (PAAS). Thus, much of the lithium in seafloor sediments is quantitatively delivered from the continents and only modified in the oceans by dilution with marine phases (Bouman et al., 2004; Chan et al., 2006).

In detail, the $Li/K_2O$ ratio in marine sediments varies by a factor of 3 (Figure 2(b)), from ~10, like average UCC (see Chapter 4.1; Teng et al., 2004), to >30, in excess of the average shale value (PAAS = 20). Such variations may occur within a single turbidite section. For example, DSDP 174 Cascadia turbidite bases (sands) have almost a factor of 2 lower $Li/K_2O$ than the turbidite tops (clays). DSDP 183 Aleutian turbidites show the same relative variation between clays and sands, but all of the values are shifted to higher overall $Li/K_2O$ (20–32). Given that these kinds of sediments are deposited rapidly and that even the clay tops lack hydrogenous components (i.e., $MnO/Al_2O_3 < 0.01$), $Li/K_2O$ likely reflects the different extents of weathering and mineralogy of their continental sources. Coarse-grained sands have lower $Li/K_2O$ than clay-rich sediments, which generally contain more weathered material. These variations are consistent with those found by Qiu et al. (2009) for Paleozoic mudrocks, where $Li/K_2O$ ratios correlate positively with the chemical index of alteration (CIA, the molar ratio of $Al_2O_3$ to the sum of $Al_2O_3 + CaO + Na_2O + K_2O$), demonstrating a control by the extent of weathering of the

**Table 1** Bulk composition of sedimentary columns subducting at trenches

| *Trench* | *N.Zealand* | *Kermadec* | *Tonga* | *Vanuatu* | *E.Sunda* | *Java* | *Sumatra* | *Andaman* | *Makran* | *Philippines* | *Ryuku* | *Nankai* | *Marianas* | *Izu-Bonin* |
|---|---|---|---|---|---|---|---|---|---|---|---|---|---|---|
| Subd rate (mm year$^{-1}$) | 27 | 65 | 160 | 81 | 70 | 65 | 47 | 30 | 35 | 67 | 71 | 30 | 40 | 41 |
| Thickness (m) | 1600 | 200 | 70 | 650 | 500 | 300 | 1400 | 3500 | 4200 | 120 | 160 | 350 | 476 | 408 |
| Density (g cm$^{-1}$) | 2.00 | 1.40 | 1.31 | 1.60 | 1.71 | 1.65 | 1.95 | 2.05 | 2.05 | 1.31 | 1.40 | 2.20 | 1.86 | 1.74 |
| %water | 30.00 | 58.00 | 62.57 | 38.35 | 34.89 | 40.30 | 24.49 | 20.17 | 20.17 | 62.57 | 58.00 | 20.00 | 23.00 | 31.57 |
| Trench length (km) | 600 | 1400 | 1350 | 1800 | 1000 | 2010 | 1000 | 1500 | 950 | 1550 | 1350 | 800 | 1400 | 1050 |
| Confidence level | 2 | 2 | 1 | 1 | 1 | 1 | 2 | 2 | 3 | 2 | 1 | 1 | 1 | 1 |
| Mass (%) | 2.7 | 0.8 | 0.5 | 6.9 | 2.9 | 2.9 | 7.1 | 19.0 | 16.8 | 0.5 | 0.7 | 1.1 | 2.8 | 1.5 |
| $SiO_2$ | 42.21 | 41.77 | 59.25 | 55.52 | 53.70 | 60.43 | 60.11 | 60.02 | 53.26 | 47.59 | 43.67 | 59.72 | 67.65 | 64.98 |
| $TiO_2$ | 0.739 | 0.429 | 0.488 | 0.520 | 0.591 | 0.710 | 0.64 | 0.62 | 0.75 | 0.50 | 0.49 | 0.61 | 0.71 | 0.29 |
| $Al_2O_3$ | 12.01 | 9.28 | 10.21 | 13.19 | 9.80 | 12.97 | 13.89 | 14.14 | 12.70 | 10.06 | 11.74 | 15.00 | 5.52 | 5.76 |
| FeO* | 6.77 | 4.55 | 7.60 | 5.08 | 4.98 | 5.94 | 5.27 | 5.09 | 6.98 | 11.37 | 12.68 | 5.23 | 4.80 | 3.17 |
| MnO | 0.15 | 0.85 | 2.21 | 0.20 | 0.36 | 0.42 | 0.49 | 0.51 | 0.64 | 0.94 | 2.71 | 0.59 | 0.21 | 0.39 |
| MgO | 5.24 | 1.89 | 2.69 | 2.77 | 2.45 | 2.72 | 2.49 | 2.42 | 3.49 | 3.09 | 3.03 | 2.22 | 3.59 | 1.63 |
| CaO | 12.55 | 15.80 | 2.12 | 7.65 | 9.06 | 2.71 | 3.35 | 3.52 | 7.37 | 7.07 | 1.48 | 3.92 | 5.04 | 7.63 |
| $Na_2O$ | 1.70 | 2.66 | 3.96 | 4.14 | 1.28 | 2.14 | 2.51 | 2.61 | 1.52 | 3.59 | 3.29 | 1.40 | 1.23 | 1.20 |
| $K_2O$ | 1.85 | 1.82 | 2.11 | 1.51 | 1.89 | 2.50 | 2.65 | 2.69 | 2.81 | 1.64 | 2.90 | 3.24 | 1.36 | 1.16 |
| $P_2O_5$ | 0.131 | 0.488 | 0.981 | 0.140 | 0.126 | 0.186 | 0.19 | 0.19 | 0.23 | 0.27 | 0.45 | 0.27 | 0.22 | 0.15 |
| $CO_2$ | 9.10 | 11.83 | 0.00 | 3.94 | 7.04 | 1.07 | 0.23 | 0.00 | 5.08 | 4.50 | 0.00 | 0.00 | 2.61 | 4.49 |
| $H_2O^+$ | 7.60 | 8.64 | 8.38 | 4.96 | 8.51 | 8.17 | 8.18 | 8.18 | 5.28 | 9.39 | 8.73 | 6.25 | 6.79 | 8.73 |
| Li | 32.13 | 47.29 | 41.80 | 31.20 | 37.77 | 49.99 | 49.43 | 49.27 | 56.12 | 60.51 | 54.62 | 49.50 | 18.70 | 47.11 |
| Be | 0.93 | 1.55 | 1.78 | 1.25 | 1.62 | 2.15 | 2.62 | 2.75 | 2.41 | 1.78 | 2.65 | 2.78 | 0.96 | 1.14 |
| B | 57.9 | 78.3 | 83.6 | 46.8 | 56.7 | 75.0 | 64.5 | 61.6 | 84.2 | 121.0 | 109.2 | 88.3 | 37.4 | 94.2 |
| Sc | 24.0 | 14.2 | 22.0 | 14.7 | 11.7 | 14.8 | 14.3 | 14.2 | 17.6 | 14.7 | 17.7 | 15.0 | 6.9 | 9.3 |
| V | 170 | 84 | 121 | 98 | 96 | 118 | 102 | 98 | 139 | 171 | 248 | 106 | 90 | 56 |
| Cr | 285 | 30.4 | 24.6 | 45.0 | 43.6 | 70.5 | 66.3 | 65.2 | 64.9 | 78.5 | 41.2 | 61.8 | 164.5 | 29.2 |
| Co | 36.8 | 84.0 | 216.9 | 17.0 | 22.6 | 25.9 | 33.2 | 35.2 | 20.4 | 43.7 | 63.4 | 15.9 | 21.6 | 20.5 |
| Ni | 101.5 | 112.7 | 251.5 | 42.0 | 63.5 | 91.5 | 75.7 | 71.3 | 98.5 | 132.2 | 172.0 | 37.8 | 99.5 | 52.3 |
| Cu | 387 | 139 | 310 | 67 | 163 | 122 | 127 | 129 | 100 | 290 | 419 | 75 | 68 | 99 |
| Zn | 115 | 82 | 62 | 42 | 82 | 100 | 89 | 86 | 113 | 125 | 239 | 92 | 64 | 72 |
| Rb | 46.8 | 55.4 | 39.2 | 22.0 | 63.3 | 82.1 | 134.4 | 148.7 | 84.4 | 38.5 | 75.7 | 140.9 | 30.3 | 46.3 |
| Cs | 2.15 | 3.17 | 2.26 | 0.76 | 3.86 | 4.94 | 8.21 | 9.11 | 4.63 | 2.55 | 5.14 | 9.52 | 1.32 | 3.00 |
| Sr | 557 | 684 | 233 | 338 | 405 | 218 | 138 | 116 | 422 | 404 | 321 | 165 | 161 | 136 |
| Ba | 577 | 1336 | 1680 | 145 | 1486 | 1068 | 561 | 423 | 851 | 483 | 556 | 540 | 311 | 884 |
| Y | 24.8 | 78.4 | 173.0 | 25.0 | 24.6 | 32.6 | 38.6 | 40.2 | 39.8 | 38.5 | 70.7 | 36.8 | 25.9 | 31.6 |
| Zr | 59 | 82 | 122 | 116 | 110 | 145 | 146 | 146 | 149 | 84 | 128 | 150 | 86 | 55 |
| Hf | 1.62 | 2.29 | 3.45 | 2.94 | 3.33 | 4.73 | 3.87 | 3.64 | 4.56 | 1.93 | 2.97 | 4.29 | 1.90 | 1.44 |
| Nb | 4.75 | 7.22 | 9.28 | 1.90 | 8.74 | 10.92 | 12.33 | 12.72 | 11.71 | 5.02 | 7.90 | 14.31 | 11.04 | 5.22 |
| Ta | 0.328 | 0.486 | 0.562 | 0.110 | 0.693 | 0.848 | 0.989 | 1.027 | 0.925 | 0.313 | 0.534 | 1.008 | 0.758 | 0.359 |
| La | 11.9 | 53.3 | 115.6 | 10.1 | 29.8 | 39.1 | 36.7 | 36.1 | 40.3 | 27.1 | 57.2 | 34.7 | 20.8 | 23.4 |
| Ce | 26.5 | 90.1 | 179.7 | 21.1 | 74.5 | 86.1 | 74.4 | 71.2 | 81.7 | 34.5 | 73.4 | 74.9 | 31.5 | 34.3 |
| Pr | 3.29 | 14.59 | 32.72 | 3.20 | 6.80 | 9.00 | 8.93 | 8.91 | 9.00 | 7.39 | 15.14 | 8.50 | 5.20 | 6.16 |
| Nd | 13.3 | 59.0 | 135.2 | 14.6 | 25.4 | 33.9 | 33.4 | 33.3 | 34.0 | 30.2 | 59.2 | 30.9 | 21.0 | 25.2 |
| Sm | 3.32 | 13.14 | 30.18 | 3.42 | 5.71 | 7.06 | 6.88 | 6.84 | 7.83 | 6.77 | 12.88 | 5.62 | 4.62 | 5.32 |
| Eu | 0.93 | 3.22 | 7.52 | 1.01 | 1.15 | 1.43 | 1.49 | 1.50 | 1.59 | 1.71 | 3.01 | 1.23 | 1.15 | 1.34 |
| Gd | 3.37 | 13.40 | 32.00 | 4.04 | 5.27 | 6.23 | 6.66 | 6.78 | 7.23 | 7.13 | 13.09 | 5.13 | 4.20 | 5.66 |
| Tb | 0.553 | 2.145 | 5.200 | 0.650 | 0.780 | 0.970 | 1.043 | 1.063 | 1.150 | 1.137 | 1.972 | 0.730 | 0.650 | 0.884 |
| Dy | 3.38 | 12.47 | 30.51 | 3.91 | 4.24 | 5.66 | 6.23 | 6.39 | 6.86 | 6.54 | 11.80 | 3.80 | 3.81 | 5.11 |
| Ho | 0.706 | 2.505 | 6.100 | 0.810 | 0.860 | 1.150 | 1.246 | 1.273 | 1.400 | 1.330 | 2.388 | 0.680 | 0.780 | 1.038 |
| Er | 1.98 | 6.91 | 16.72 | 2.29 | 2.49 | 3.35 | 3.42 | 3.44 | 4.03 | 3.65 | 6.61 | 1.75 | 2.12 | 2.82 |
| Yb | 1.95 | 6.08 | 14.50 | 2.73 | 2.43 | 3.24 | 3.33 | 3.36 | 3.93 | 3.26 | 5.86 | 1.60 | 1.86 | 2.53 |
| Lu | 0.297 | 0.936 | 2.228 | 0.380 | 0.386 | 0.500 | 0.511 | 0.514 | 0.600 | 0.498 | 0.887 | 0.250 | 0.268 | 0.388 |
| Pb | 7.4 | 29.5 | 62.1 | 7.7 | 34.6 | 33.4 | 26.6 | 24.7 | 27.7 | 69.2 | 89.8 | 33.4 | 7.4 | 15.4 |
| Th | 3.36 | 6.43 | 6.59 | 1.37 | 7.73 | 9.78 | 12.19 | 12.85 | 10.31 | 3.04 | 7.40 | 14.20 | 2.62 | 4.39 |
| U | 1.14 | 1.77 | 1.79 | 0.45 | 0.99 | 1.47 | 2.21 | 2.41 | 1.25 | 1.17 | 2.22 | 0.99 | 0.58 | 0.92 |
| $\delta^7$Li | 4.7 | 4.3 | 7.3 | 4.4 | 0.3 | 2.9 | 2.1 | 1.9 | 0.9 | 3.7 | 5.9 | 2.6 | 9.3 | 6.2 |
| $^{87}Sr/^{86}Sr$ | 0.70928 | 0.71014 | 0.70952 | 0.70548 | 0.71682 | 0.71682 | 0.72969 | 0.73631 | 0.71109 | | | | 0.70617 | 0.70956 |
| $^{143}Nd/^{144}Nd$ | 0.51259 | 0.51235 | 0.51234 | 0.51291 | 0.51216 | 0.51216 | 0.51200 | 0.51195 | 0.51203 | 0.51245 | 0.51238 | 0.51238 | 0.51252 | 0.51234 |
| $^{206}Pb/^{204}Pb$ | 18.891 | 18.801 | 18.763 | 18.644 | 18.990 | 18.990 | 19.231 | 19.320 | 18.610 | | 18.604 | | 18.917 | 18.589 |
| $^{207}Pb/^{204}Pb$ | 15.636 | 15.663 | 15.666 | 15.574 | 15.741 | 15.741 | 15.791 | 15.810 | 15.600 | | 15.664 | | 15.646 | 15.587 |
| $^{208}Pb/^{204}Pb$ | 38.754 | 38.803 | 38.784 | 38.445 | 39.328 | 39.328 | 39.644 | 39.760 | 38.800 | | 38.722 | | 38.918 | 38.558 |

Oxides in wt%; all others in ppm. Trench lengths from von Huene and Scholl (1991) and subduction velocities (orthogonal to the trench) from Syracuse and Abers (2006). See

source. Such detrital variations overwhelm those created in the oceans; hydrogenous and biogenic sediments fall almost exclusively within the range of terrigenous clays and turbidites in terms of $Li/K_2O$.

Li isotopes in marine sediments fall within the end-members of the UCC ($\delta^7Li = 0 \pm 2‰$; Teng et al., 2004) and seawater ($\delta^7Li \sim +31‰$; Chan and Edmond, 1988). Within the terrigenous clays and turbidites that show the full range of $Li/K_2O$, there is a systematic increase in $\delta^7Li$ (from +1 to +5‰) with decreasing $Li/K_2O$ and decreasing CIA (**Figure 2(c)**). Again, this likely reflects the extent of weathering and mineralogy of the different continental source regions, where greater weathering correlates with a higher CIA and lower $\delta^7Li$. Such a relationship was identified by Qiu et al. (2009) for Paleozoic mudrocks, which generally extend to lighter Li and greater CIA than most marine sediments. Notably, high-CIA shales (such as PAAS) possess negative $\delta^7Li$ on average, while many marine turbidites possess positive $\delta^7Li$ due to a greater proportion of juvenile material. Thus, detrital sediments show strong correlations between Li isotopes, abundances, and weathering indices. In contrast, hydrogenous and biogenic phases generally record much heavier $\delta^7Li$: +6 to +10‰ in Tonga hydrogenous clays; +5 to +12‰ in Central American and Sunda nannofossil/foram oozes; and +5 to +15‰ in Marianas

| Japan | Kurile | Kamchatka | Aleutians | Alaska | Cascadia | Mexico | CentAm | Colombia | Peru | Chile-35° | Chile-40° | Chile-45° | Sandwich | N.Antilles | S. Antilles |
|---|---|---|---|---|---|---|---|---|---|---|---|---|---|---|---|
| 82 | 78 | 75 | 60 | 53 | 35 | 52 | 70 | 59 | 76 | 72 | 75 | 75 | 62 | 18 | 18 |
| 285 | 345 | 435 | 350 | 780 | 900 | 170 | 425 | 290 | 125 | 1000 | 1200 | 1500 | 200 | 235 | 1750 |
| 1.58 | 1.64 | 1.70 | 1.64 | 1.80 | 1.88 | 1.37 | 1.62 | 1.44 | 1.47 | 1.88 | 1.88 | 1.88 | 1.49 | 1.66 | 1.88 |
| 42.68 | 38.80 | 35.15 | 41.54 | 32.40 | 30.00 | 59.01 | 48.69 | 53.04 | 50.00 | 30.00 | 30.00 | 30.00 | 50.00 | 37.30 | 30.00 |
| 800 | 1650 | 550 | 1900 | 800 | 1300 | 1450 | 1450 | 1050 | 1500 | 495 | 550 | 275 | 800 | 400 | 400 |
| 2 | 2 | 2 | 1 | 1 | 1 | 1 | 1 | 3 | 2 | 2 | 2 | 2 | 1 | 2 | 2 |
| 1.2 | 3.3 | 1.5 | 2.8 | 3.0 | 4.0 | 0.5 | 2.7 | 0.9 | 0.8 | 3.5 | 4.8 | 3.0 | 0.5 | 0.1 | 1.2 |
| 65.43 | 66.15 | 71.40 | 59.63 | 60.98 | 62.78 | 54.24 | 23.39 | 25.94 | 25.14 | 56.11 | 56.93 | 59.36 | 66.46 | 51.90 | 59.73 |
| 0.37 | 0.32 | 0.26 | 0.73 | 0.78 | 0.69 | 0.57 | 0.17 | 0.18 | 0.17 | 0.91 | 0.91 | 0.92 | 0.55 | 0.58 | 0.67 |
| 8.76 | 7.85 | 6.50 | 13.86 | 15.10 | 13.66 | 13.13 | 3.31 | 3.53 | 4.17 | 16.29 | 16.35 | 16.59 | 11.54 | 15.50 | 11.66 |
| 3.81 | 3.56 | 2.61 | 5.61 | 7.24 | 5.43 | 11.04 | 3.77 | 3.84 | 4.32 | 6.59 | 6.62 | 6.45 | 4.96 | 5.99 | 4.62 |
| 0.39 | 0.40 | 0.20 | 0.15 | 0.23 | 0.06 | 2.33 | 0.43 | 0.44 | 0.67 | 0.14 | 0.12 | 0.11 | 0.10 | 0.26 | 0.08 |
| 1.87 | 1.54 | 1.32 | 2.71 | 3.24 | 2.53 | 2.87 | 1.52 | 1.57 | 1.84 | 3.04 | 3.05 | 3.11 | 2.25 | 2.36 | 1.91 |
| 3.23 | 0.61 | 0.82 | 3.41 | 2.08 | 3.80 | 1.73 | 34.59 | 32.15 | 32.14 | 4.61 | 4.60 | 4.83 | 1.10 | 3.21 | 1.00 |
| 2.30 | 2.82 | 3.11 | 3.61 | 2.96 | 2.74 | 2.50 | 0.83 | 1.02 | 1.95 | 3.87 | 3.64 | 3.53 | 2.65 | 1.79 | 2.54 |
| 1.72 | 1.57 | 1.43 | 2.11 | 2.22 | 2.71 | 1.23 | 0.68 | 0.71 | 0.97 | 1.73 | 1.76 | 2.10 | 2.43 | 1.81 | 1.84 |
| 0.14 | 0.20 | 0.11 | 0.15 | 0.18 | 0.16 | 0.36 | 0.20 | 0.21 | 0.30 | 0.19 | 0.18 | 0.22 | 0.15 | 0.16 | 0.34 |
| 1.70 | 0.00 | 0.00 | 0.00 | 0.00 | 0.00 | 0.00 | 26.55 | 25.26 | 24.53 | 0.00 | 0.00 | 1.50 | 0.00 | 1.73 | 0.00 |
| 10.18 | 14.83 | 12.18 | 8.02 | 5.00 | 5.42 | 10.00 | 4.59 | 5.17 | 3.94 | 6.49 | 5.81 | 1.50 | 7.81 | 14.29 | 14.93 |
| 43.02 | 32.44 | 22.24 | 55.21 | 50.45 | 40.71 | 71.31 | 29.39 | 32.61 | 29.26 | 37.47 | 40.92 | 52.38 | 44.36 | 59.91 | 38.32 |
| 1.46 | 1.31 | 1.33 | 1.69 | 1.66 | 2.32 | 2.25 | 0.73 | 0.81 | 1.14 | 1.48 | 1.52 | 1.80 | 2.44 | 1.55 | 1.59 |
| 86.0 | 64.9 | 44.5 | 82.8 | 75.7 | 61.1 | 142.6 | 58.8 | 65.2 | 58.5 | 58.9 | 62.9 | 78.6 | 112.0 | 89.9 | 57.5 |
| 11.8 | 11.4 | 11.0 | 17.6 | 18.6 | 14.4 | 15.7 | 7.2 | 7.5 | 9.6 | 17.8 | 17.7 | 17.1 | 16.3 | 11.7 | 13.7 |
| 77 | 79 | 61 | 145 | 151 | 108 | 193 | 60 | 63 | 70 | 149 | 161 | 141 | 95 | 239 | 189 |
| 35.1 | 35.2 | 30.7 | 69.2 | 84.2 | 76.7 | 97.1 | 14.6 | 15.3 | 41.6 | 79.5 | 68.3 | 57.2 | 44.0 | 69.0 | 80.3 |
| 22.7 | 29.1 | 23.8 | 26.0 | 17.6 | 13.7 | 36.0 | 16.5 | 17.3 | 42.4 | 24.1 | 20.9 | 16.5 | 17.6 | 22.7 | 22.8 |
| 55.2 | 63.0 | 50.4 | 46.0 | 46.2 | 37.1 | 127.2 | 86.0 | 89.2 | 120.3 | 73.1 | 52.4 | 30.1 | 53.8 | 73.6 | 58.1 |
| 92 | 84 | 96 | 65 | 74 | 32 | 287 | 134 | 136 | 293 | 140 | 93 | 34 | 101 | 117 | 92 |
| 80 | 72 | 72 | 86 | 118 | 80 | 243 | 118 | 122 | 154 | 106 | 92 | 94 | 117 | 124 | 98 |
| 60.9 | 55.5 | 46.8 | 66.1 | 78.5 | 94.3 | 83.3 | 15.6 | 16.1 | 37.4 | 52.4 | 47.7 | 71.8 | 101.5 | 66.7 | 67.0 |
| 4.77 | 4.62 | 2.99 | 3.69 | 4.05 | 4.06 | 5.41 | 0.72 | 0.76 | 2.86 | 3.54 | 2.70 | 3.83 | 6.21 | 5.09 | 3.80 |
| 116 | 80 | 87 | 245 | 227 | 323 | 214 | 1227 | 1263 | 1025 | 339 | 320 | 296 | 151 | 110 | 150 |
| 820 | 575 | 770 | 2074 | 1475 | 768 | 2750 | 2571 | 2692 | 2480 | 633 | 513 | 432 | 1476 | 230 | 200 |
| 28.5 | 28.0 | 18.6 | 21.6 | 24.6 | 26.6 | 44.6 | 26.3 | 27.2 | 51.5 | 18.9 | 19.1 | 26.2 | 25.2 | 26.1 | 22.2 |
| 80 | 77 | 67 | 131 | 135 | 207 | 97 | 45 | 49 | 72 | 129 | 136 | 145 | 101 | 104 | 138 |
| 2.13 | 1.94 | 1.59 | 3.26 | 3.54 | 5.19 | 2.13 | 0.96 | 1.04 | 1.28 | 3.22 | 3.41 | 3.61 | 2.70 | 2.79 | 3.56 |
| 7.08 | 7.19 | 4.59 | 8.43 | 9.77 | 17.08 | 8.65 | 1.99 | 2.16 | 3.71 | 4.72 | 4.74 | 8.83 | 8.31 | 11.82 | 10.82 |
| 0.381 | 0.295 | 0.269 | 0.557 | 0.650 | 1.092 | 0.586 | 0.132 | 0.144 | 0.265 | 0.345 | 0.346 | 0.582 | 0.569 | 0.819 | 0.748 |
| 22.5 | 20.9 | 14.6 | 18.0 | 20.0 | 34.9 | 36.3 | 14.0 | 14.6 | 28.6 | 15.3 | 14.9 | 20.9 | 25.5 | 33.4 | 25.6 |
| 41.8 | 47.0 | 34.3 | 39.0 | 42.0 | 68.4 | 25.4 | 11.3 | 11.8 | 23.2 | 35.0 | 33.9 | 45.9 | 58.9 | 80.6 | 50.5 |
| 6.09 | 5.33 | 3.62 | 4.82 | 5.50 | 8.14 | 8.34 | 3.43 | 3.57 | 6.29 | 4.26 | 4.18 | 5.529 | 6.47 | 8.16 | 5.99 |
| 24.2 | 21.0 | 14.4 | 19.1 | 21.7 | 30.4 | 34.1 | 13.5 | 14.1 | 25.4 | 17.7 | 17.4 | 21.9 | 25.8 | 30.6 | 22.6 |
| 5.35 | 5.27 | 3.40 | 4.43 | 4.84 | 5.85 | 7.00 | 2.92 | 3.04 | 5.62 | 3.99 | 3.94 | 4.753 | 5.22 | 6.04 | 4.43 |
| 1.25 | 1.19 | 0.77 | 1.10 | 1.30 | 1.34 | 1.88 | 0.72 | 0.75 | 1.49 | 1.05 | 1.05 | 1.164 | 1.29 | 1.27 | 0.99 |
| 5.18 | 4.83 | 3.38 | 4.31 | 4.45 | 5.16 | 7.57 | 3.33 | 3.46 | 6.10 | 3.83 | 3.79 | 4.365 | 4.97 | 5.15 | 3.84 |
| 0.824 | 0.757 | 0.524 | 0.700 | 0.730 | 0.782 | 1.189 | 0.560 | 0.582 | 1.009 | 0.583 | 0.589 | 0.679 | 0.843 | 0.821 | 0.611 |
| 4.82 | 4.37 | 3.03 | 4.12 | 4.40 | 4.41 | 7.07 | 3.43 | 3.57 | 6.67 | 3.54 | 3.64 | 3.977 | 4.51 | 4.55 | 3.49 |
| 1.008 | 0.936 | 0.638 | 0.850 | 0.870 | 0.892 | 1.475 | 0.737 | 0.766 | 1.507 | 0.715 | 0.734 | 0.795 | 0.919 | 0.926 | 0.730 |
| 2.83 | 2.70 | 1.79 | 2.30 | 2.45 | 2.53 | 4.14 | 2.12 | 2.20 | 4.36 | 2.08 | 2.16 | 2.3377 | 2.55 | 2.63 | 2.10 |
| 2.66 | 2.70 | 1.81 | 2.20 | 2.30 | 2.45 | 3.91 | 2.06 | 2.15 | 4.10 | 2.01 | 2.06 | 2.1146 | 2.42 | 2.44 | 2.00 |
| 0.407 | 0.413 | 0.283 | 0.338 | 0.361 | 0.386 | 0.628 | 0.323 | 0.336 | 0.655 | 0.304 | 0.313 | 0.330 | 0.391 | 0.374 | 0.310 |
| 23.3 | 22.0 | 13.8 | 13.1 | 12.7 | 13.8 | 38.9 | 7.4 | 9.8 | 19.1 | 15.7 | 13.0 | 12.9 | 22.0 | 18.7 | 11.5 |
| 6.05 | 5.76 | 4.15 | 5.49 | 5.87 | 10.29 | 6.00 | 0.93 | 1.21 | 3.54 | 5.08 | 4.74 | 6.693 | 9.43 | 10.88 | 7.69 |
| 1.40 | 1.29 | 1.21 | 2.39 | 1.95 | 2.74 | 2.91 | 1.37 | 2.97 | 1.26 | 1.98 | 1.98 | 1.84 | 1.62 | 1.39 | 4.90 |
| 4.1 | 2.7 | 4.0 | 2.0 | 1.9 | 2.2 | 1.6 | 5.6 | 9.4 | 7.1 | 3.3 | 3.3 | 2.4 | 3.4 | -0.4 | -1.1 |
| 0.71039 | 0.71125 | 0.71088 | 0.70635 | 0.70588 | 0.71490 | 0.70847 | 0.70852 | | | 0.70493 | 0.70539 | 0.70770 | 0.70919 | 0.71585 | 0.71083 |
| 0.51232 | 0.51234 | 0.51243 | 0.51263 | 0.51261 | 0.51216 | 0.51253 | 0.51252 | 0.51248 | 0.51248 | 0.51275 | 0.51273 | 0.51253 | 0.51228 | 0.51197 | 0.51202 |
| 18.795 | 18.813 | 18.775 | 19.042 | 18.940 | 19.136 | 18.638 | 18.459 | | | 18.610 | 18.632 | 18.702 | 18.649 | 19.315 | 19.492 |
| 15.664 | 15.694 | 15.690 | 15.626 | 15.614 | 15.677 | 15.585 | 15.515 | | | 15.621 | 15.622 | 15.629 | 15.633 | 15.767 | 15.763 |
| 38.786 | 38.885 | 38.882 | 38.686 | 38.641 | 39.140 | 38.344 | 38.166 | | | 38.559 | 38.575 | 38.705 | 38.501 | 39.347 | 39.213 |

Appendix A for all details and references, and supplementary Table A for some individual trench lithologies. Confidence levels: 1 = highest confidence; 4 = lowest.

radiolarite and porcellanites (Bouman et al., 2004; Chan et al., 2006). Because neither their Li concentrations nor $Li/K_2O$ ratios reflect simple uptake of seawater, the heavy Li in hydrogenous and biogenic phases likely reflects, instead, seawater or pore water exchange. Thus, Li isotopes and concentrations may be coupled in terrigenous sediments, but not in biogenic or authigenic marine phases.

### 4.17.3.7 Beryllium

The systematics of Be in marine sediments is simpler than that of Li, and for most sediments, Be correlates strongly with alkali metals and other detritally controlled elements. Notably, Be does not behave like the other alkaline earth elements, such as Ca, Mg, or Sr, and is too small to substitute in the carbonate structure. Figure 2(d) shows a strong correlation between Be and $K_2O$ in most classes of sediments – terrigenous clays, turbidites, biogenic carbonates, and siliceous oozes. Indeed, marine sediments have a common $Be/K_2O$ ratio of $0.86 \pm 0.04$ ppm per wt% (2 sigma on the mean of a Gaussian distribution) that is equivalent to the UCC ratio, within its uncertainty ($0.74 \pm 0.3$; see Chapter 4.1). On the other hand, the alluvial sediments reported in Kamber et al. (2005) systematically increase in $Be/K_2O$, from 0.8 to 2.0, with

**Table 2** New global subducting sediment (GLOSS-II) composition

| | *GLOSS-II* | ± | *GLOSS* |
|---|---|---|---|
| $SiO_2$ | 56.60 | 3.0 | 58.57 |
| $TiO_2$ | 0.64 | 0.04 | 0.62 |
| $Al_2O_3$ | 12.51 | 0.69 | 11.91 |
| FeO* | 5.67 | 0.33 | 5.21 |
| MnO | 0.43 | 0.03 | 0.32 |
| MgO | 2.75 | 0.16 | 2.48 |
| CaO | 6.22 | 0.33 | 5.95 |
| $Na_2O$ | 2.50 | 0.12 | 2.43 |
| $K_2O$ | 2.21 | 0.14 | 2.04 |
| $P_2O_5$ | 0.20 | 0.01 | 0.19 |
| $CO_2$ | 3.07 | 0.23 | 3.01 |
| $H_2O^+$ | 7.09 | 0.35 | 7.29 |
| Li | 44.8 | 2.8 | |
| Be | 1.99 | 0.13 | |
| B | 67.9 | 4.0 | |
| Sc | 15.0 | 0.83 | 13.1 |
| V | 116 | 6.3 | 110 |
| Cr | 68.8 | 3.7 | 78.9 |
| Co | 26.9 | 1.3 | 21.9 |
| Ni | 73.0 | 4.6 | 70.5 |
| Cu | 116 | 5.9 | 75 |
| Zn | 93.0 | 5.2 | 86.4 |
| Rb | 83.7 | 5.7 | 57.2 |
| Cs | 4.90 | 0.33 | 3.48 |
| Sr | 302 | 17.2 | 327 |
| Ba | 786 | 39.0 | 776 |
| Y | 33.3 | 2.0 | 29.8 |
| Zr | 129 | 7.6 | 130 |
| Hf | 3.42 | 0.22 | 4.06 |
| Nb | 9.42 | 0.64 | 8.94 |
| Ta | 0.698 | 0.049 | 0.630 |
| La | 29.1 | 2.0 | 28.8 |
| Ce | 57.6 | 4.0 | 57.3 |
| Pr | 7.15 | 0.46 | |
| Nd | 27.6 | 1.7 | 27.0 |
| Sm | 6.00 | 0.38 | 5.78 |
| Eu | 1.37 | 0.08 | 1.31 |
| Gd | 5.81 | 0.36 | 5.26 |
| Tb | 0.92 | 0.06 | |
| Dy | 5.43 | 0.33 | 4.99 |
| Ho | 1.10 | 0.07 | |
| Er | 3.09 | 0.19 | 2.92 |
| Yb | 3.01 | 0.19 | 2.76 |
| Lu | 0.459 | 0.03 | 0.413 |
| Pb | 21.2 | 1.4 | 19.9 |
| Th | 8.10 | 0.59 | 6.91 |
| U | 1.73 | 0.09 | 1.68 |
| $\delta^7Li$ | 2.42 | 0.18 | |
| $^{87}Sr/^{86}Sr$ | 0.71236 | 0.00033 | 0.7173 |
| $^{143}Nd/^{144}Nd$ | 0.51221 | 0.00002 | 0.51218 |
| $^{206}Pb/^{204}Pb$ | 18.929 | 0.025 | 18.913 |
| $^{207}Pb/^{204}Pb$ | 15.694 | 0.007 | 15.673 |
| $^{208}Pb/^{204}Pb$ | 39.121 | 0.028 | 38.899 |

Oxides in wt%, others in ppm. GLOSS-II uncertainty is calculated from a Monte Carlo scheme, whereby each trench is allowed to vary randomly within its uncertainty, assuming 10% uncertainty for all elements from confidence level 1 trenches, 20% for confidence level 2, etc. The uncertainty reported is the maximum difference in the global weighted mean for 90 out of 100 trials.

increasing CIA, demonstrating fractionation of Be from $K_2O$ during weathering. However, virtually all of these sediments have a CIA>70, while virtually all of the marine sediments plotted in Figure 2(d) have a CIA<70, and so advanced stages of weathering are not as well represented in the marine realm. This supports the notion that Be and $K_2O$ are not fractionated during moderate weathering, transport, deposition or diagenesis of rapidly deposited sediments. If this is true, then it may be possible to use the coherent marine sediment record to provide a more robust estimate of the average UCC. The current uncertainty on the Be concentration of the UCC is $2.1 \pm 0.9$ ppm, or 40% (see Chapter 4.1). Using the marine sediment $Be/K_2O$ ratio and the better constrained UCC $K_2O$ ($2.8 \pm 0.23$), a new Be estimate for the UCC is $2.4 \pm 0.2$ ppm. This overlaps, but is considerably better constrained than, the previous estimate.

While most sediments record the continental $Be/K_2O$ ratio, hydrogenous and hydrothermal sediments do not. In these sediments, ratios can be higher and lower than the UCC value, even within the same sedimentary section (e.g., DSDP 294/295 Ryukyu). Some authigenic sediments apparently take up Be from seawater, and the highest Be concentrations in marine sediments (>4 ppm) are found in brown to black metalliferous clays and Mn nodules. Such concentrations have been useful in the $^{10}Be$ dating of Mn crusts. While Be uptake is responsible for some of the variation in $Be/K_2O$ in hydrogenous sediments, just as important is the apparent fractionation during authigenic formation of different clay minerals and zeolites, which may enhance $K_2O$ instead.

### 4.17.3.8 Boron

Mostly a by-product of isotope studies, boron concentrations are still not measured routinely in bulk marine sediments. Ishikawa and Nakamura (1993) measured boron isotopes and concentrations in a wide variety of sediment types, from clays to chert and loess, and their study remains one of the most useful for boron. Other studies examined B and Li together (Chan et al., 2006; You et al., 1995), while Karl et al. (1992) measured B in Marianas sediments from ODP Leg 129, with an unusually complete set of multielement analyses. These studies are the basis for this preliminary assessment of boron in marine sediments. Only Karl et al.'s (1992) study provides any major element data with which to place B in context, and yet all studies also provide Li analyses, so this is the comparative element in Figure 3. Biogenic carbonates and cherts have the lowest B concentrations (ODP 801 cherts; Vengosh et al., 1991), consistent with boron's host primarily in the detrital phase. Detrital sediments from individual sites often possess a characteristic Li/B ratio (e.g., Cascadia turbidites and ODP 808 Shikoku Basin sediments), which varies between sites. Almost all marine sediments have significantly higher B concentrations than the UCC estimate (20 ppm) and loess (30 ppm; Ishikawa and Nakamura, 1993). Except for a single clay layer from a turbidite, all marine sediments have higher B/Li ratios than UCC (0.7), and range up to ~2. Whether this is just regional, but poorly sampled variability in the continental detritus, or a real offset between igneous-dominated UCC values and weathered continental detritus awaits additional data.

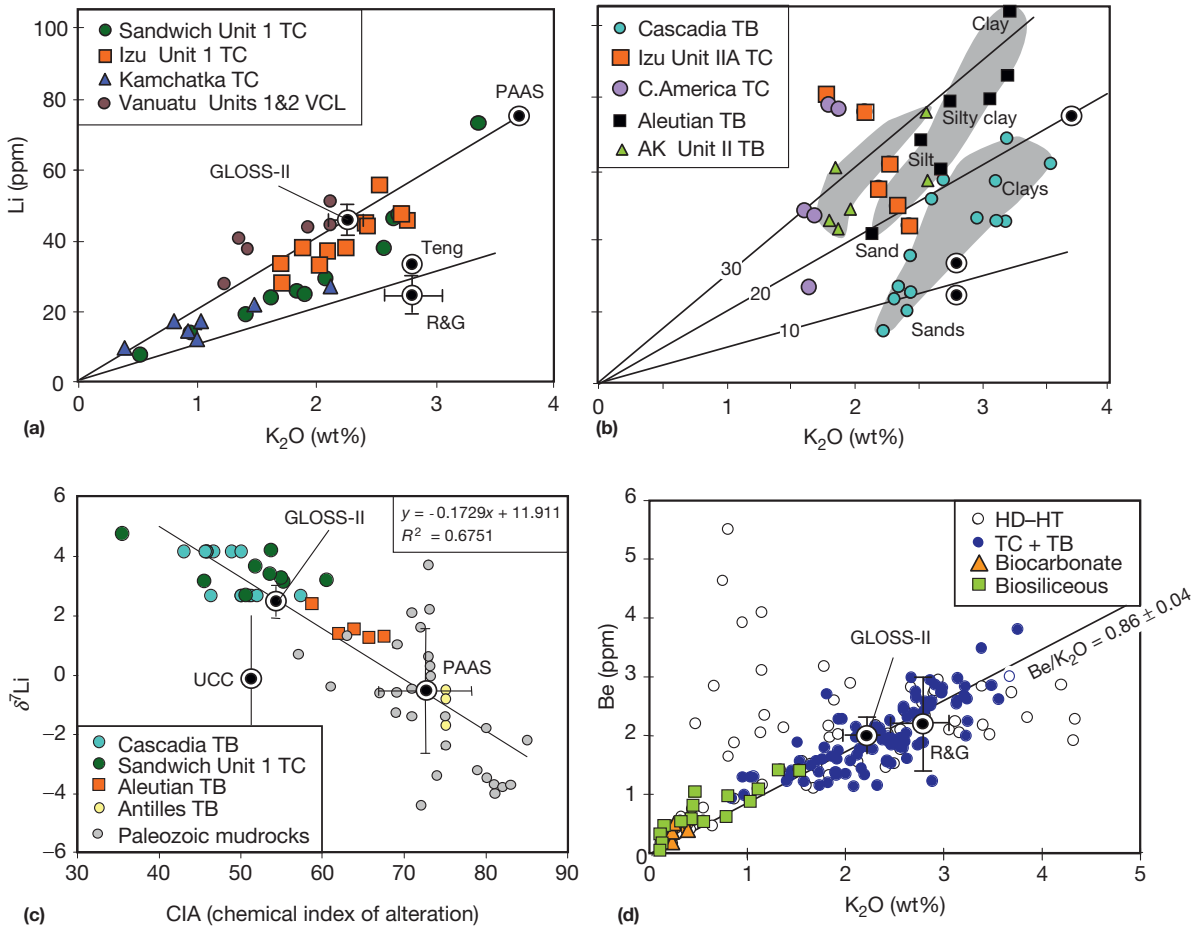


**Figure 2** Variation in Li, Be, and Li isotopes versus $K_2O$ in marine sediments (data from Vervoort et al., 2011, except as noted below). Hydrogenous (HD)–hydrothermal (HT), terrigenous clays (TC), biocarbonate, biosiliceous, and volcaniclastic (VCL) designations as in Vervoort et al. (2011). (a) Sediments with Li/$K_2O$ similar to upper crustal averages from Rudnick and Gao (see **Chapter 4.1**) and Teng et al. (2004) and PAAS from Taylor and McLennan (1985). Izu sediments (ODP 1149) from Plank et al. (2007). (b) Turbidites (TB) and terrigenous clays (TC) that vary in Li/$K_2O$ from 10 to 30. Within each turbidite unit, Li/$K_2O$ decreases with increasing grain size (from clay to sand). (c) Inverse relationship between $\delta^7$Li and CIA (CIA = molar ratio of $Al_2O_3/(Al_2O_3 + CaO + Na_2O + K_2O)$), after Qiu et al. (2009). Cascadia data include CIA from DSDP Site 174 (Prytulak et al., 2006) plotted at Li isotope average for sands and clays from ODP Site 1027 (Chan et al., 2006). Antilles Li isotope data from DSDP 543 (Bouman et al., 2004), plotted at CIA for Unit 5 sediments with similar Li concentrations from Carpentier et al. (2009). South Sandwich and Aleutian Li isotope data from Chan et al. (2006). PAAS is calculated as average of shales in Teng et al. (2004). Paleozoic mudrocks from the British Caledonides from Qiu et al. (2009). Upper continental crust (UCC) is from Teng et al. (2004) and Rudnick and Gao (see **Chapter 4.1**). (d) Terrigenous clays and turbidites and biogenic sediments define a Be/$K_2O$ ratio of $0.86 \pm 0.04$, identical to the upper crustal average of Rudnick and Gao (see **Chapter 4.1**). HD and HT sediments are more scattered, more enriched in Be relative to $K_2O$. Locations refer to drill core samples from ODP 701 (South Sandwich), ODP 881 (Kamchatka), DSDP 286 (Vanuatu), DSDP 178 (Alaska), DSDP 495 (Central America), DSDP 183 (Aleutian), and DSDP 174 (Cascadia) sediments from Vervoort et al. (2011).

### 4.17.3.9 Niobium and Tantalum Revisited

With an order of magnitude more data available in the last decade, Nb concentrations can be shown to correlate with $K_2O$ (**Figure 4(a)**). These elements otherwise have distinct geochemical behavior, but they behave coherently in marine sediments because they are largely tied to the detrital phase and diluted by biogenic silica or carbonate. Nb is not strongly taken up in hydrogenous phases (with the exception of some Mn nodules, which may have very high Nb, >50 ppm). Moreover, the UCC Nb/$K_2O$ ratio, which has been revised dramatically (Nb decreasing from 25, Taylor and McLennan, 1985, to 12, see **Chapter 4.1**), now conforms well to that in marine sediments. The revisions to UCC were in part motivated by the strong offset in marine sediments (Plank and Langmuir, 1998), and while the new UCC estimate of Rudnick and Gao (see **Chapter 4.1**) includes marine sediments in the average, other independent assessments (from juvenile crustal domains: Condie, 1993; loess and continental shales: Barth et al., 2000; and East China crustal composites: Gao et al., 1998) support the lower Nb concentrations. Most marine sediments have Nb/$K_2O$ similar to UCC, although in detail, different regions have slightly different ratios, as shown by the linear arrays in **Figure 4(a)**. The DSDP 174 Cascadia turbidites have distinctly higher Nb (and Nb/Ta, see below) than other sediments; this is not due to heavy mineral concentration, as

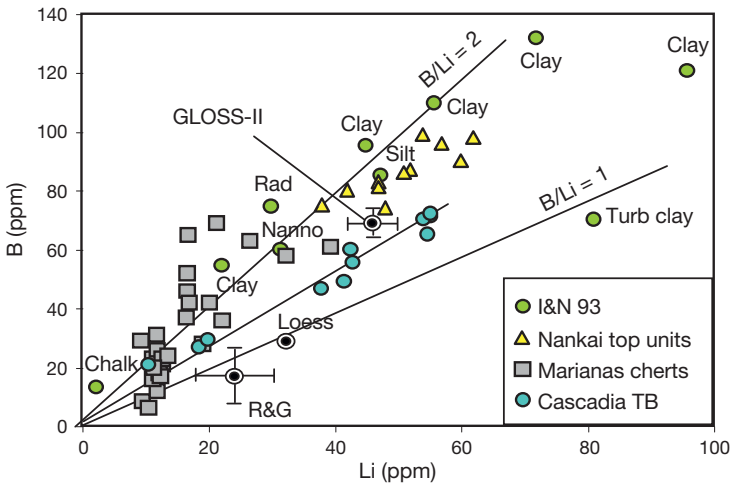


**Figure 3** Boron and Li contents of marine sediments. Most possess B/Li ratios between 1 and 2, in excess of upper continental crust (Rudnick and Gao, 2012) and China loess (Ishikawa and Nakamura, 1993). Data sources: DSDP 174 (Cascadia) turbidites from Chan et al. (2006) and Vervoort et al. (2011); ODP 801 (Marianas) cherts from Karl et al. (1992); ODP 808 (Nankai) sediments, mostly trench turbidites, above the decollement zone, from You et al. (1995); and various marine sediments, labeled by type, from Ishikawa and Nakamura (1993).

the sandy turbidite bases (which concentrate these phases) do not have any higher Nb/$K_2O$ than the clay-rich tops. Moreover, other turbidite sections have lower Nb/$K_2O$ than UCC (e.g., DSDP 183–Aleutians), and so high Nb is not a feature inherent to turbidites, but instead, must characterize the Proterozoic continental sources that supply Cascadia turbidites (Prytulak et al., 2006).

Nb and Ta are sister elements that strongly covary, leading to a limited range in their ratio in most rocks on Earth (Nb/Ta = 11–17; Munker et al., 2003). It is notable, however, that this limited range in the Nb/Ta ratio is uniformly lower in all major terrestrial reservoirs than in average chondrites (i.e., 17.4–19.9; Jochum et al., 2000; Munker et al., 2003), and this observation has led to considerable debate in the literature as to its origin (Kamber et al., 2003; McDonough, 1991; Munker et al., 2003; Nebel et al., 2010; Rudnick et al., 2000; Wade and Wood, 2001). The abundance of ICP-MS analyses of marine sediments motivates a new look at their Nb/Ta ratios, as this technique affords comeasurement of Nb and Ta in the same sample aliquot, unlike most prior methods (i.e., commonly Nb by X-ray fluorescence and Ta by neutron activation. although both were measured by the less common spark source mass spectrometry method). There is no doubt that there are real regional variations in the Nb/Ta ratio in marine sediments (**Figure 4(b)**). This is especially clear in turbidite samples, which derive from more regional sources (i.e., drained by large rivers). For example, DSDP 174 Cascadia turbidites and DSDP 211 Nicobar Fan turbidites are completely distinct in their average Nb/Ta ratios, at $15.7 \pm 0.6$ and $12.2 \pm 1.1$, respectively. In a dedicated study of the rivers in the Murray–Darling Basin of Australia, Marx and Kamber (2010) found that sediments in each river, even in each tributary, may have a distinct Nb/Ta ratio. Authigenic processes may also fractionate Nb somewhat from Ta, as some hydrogenous clays have high Nb/Ta ratios (DSDP 596 Tonga clays possess Nb/Ta up to 19). On the other hand, terrigenous clays contain minor hydrogenous phases and derive from larger continental source volumes than turbidites and so should provide the best estimate of the UCC. Indeed, the average of 50 terrigenous clays from seven different sites yields a well-defined Nb/Ta ratio of $14 \pm 1$ (1 standard deviation) $\pm 0.3$ (two sigma on the mean). This value is within uncertainty the same as GLOSS ($14.2 \pm 2$) and prior UCC estimates ($12.5 \pm 1.8$, Barth et al., 2000; and $13.4 \pm 1.85$, see **Chapter 4.1**) but is now more precisely defined. The larger uncertainties in these other estimates likely reflect real regional variations (E. China Nb/Ta = 16, Gao et al., 1998; Australian shales = 12.1, Barth et al., 2000), which may be better averaged in marine sediments. The terrigenous clay average here is remarkably similar to MUQ (MUd from Queensland), an average of 25 rivers in E. Australia (Nb/Ta = $13.77 \pm 1.08$; Kamber et al., 2005). In that study, it was clear that the Nb/Ta ratio in alluvial sediments reflects mixing between a low continental ratio (approaching 12) and a higher ratio typical of mafic igneous rocks (>15). Such mixing of old and mafic juvenile material on the continents will contribute to the local variability in marine sediments. Finally, the marine terrigenous Nb/Ta ratio is identical to the estimate of Munker et al. (2003) for the bulk silicate earth (both $14 \pm 0.3$, two sigma), although as with chondrites, there is yet considerable uncertainty in bulk earth Nb/Ta (i.e., the canonical ratio is $17.8 \pm 3.8$ in McDonough and Sun, 1995).

### 4.17.3.10 Lead

In hydrothermal sediments, Pb concentrations may be as high as 250 ppm and Pb isotopes reflect mid-ocean ridge basalt (MORB) sources (Barrett et al., 1987). In hydrogenetic sediments, Pb concentrations may reach 1000 ppm and isotopes reflect seawater sources (Aplin and Cronan, 1985; van de Flierdt et al., 2003). Lead may be associated with both Fe oxide and Mn oxide phases in ferromanganese marine sediments (Takahashi et al., 2007), although Koschinsky and Hein (2003) argue that negatively charged Pb carbonate complexes should be bound to the weakly positively charged surface of the amorphous FeOOH phase. Indeed, there does seem to be a strong relationship between Pb and FeO in both hydrothermal

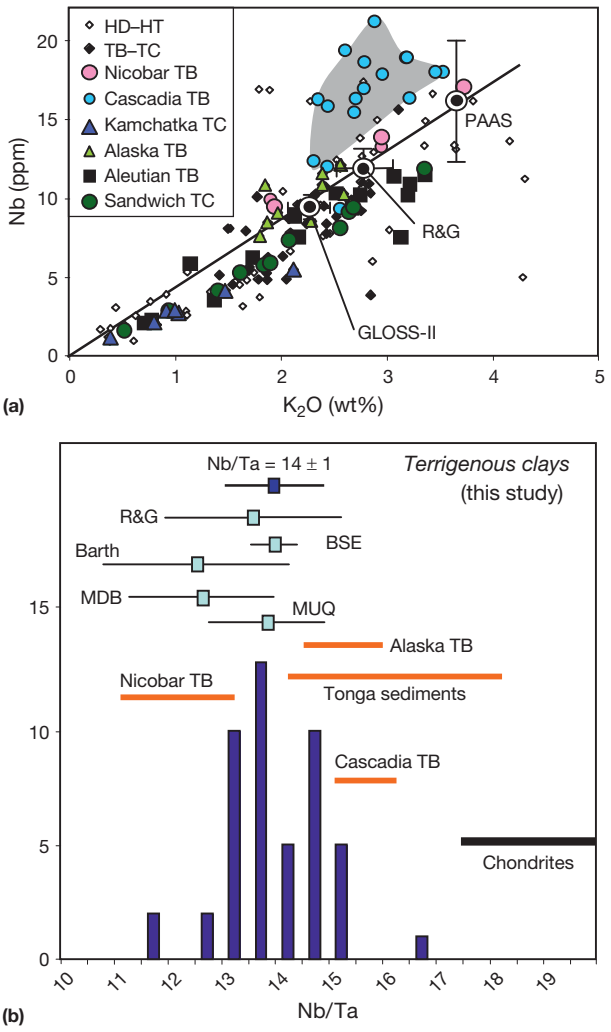


**Figure 4** Nb systematics in marine sediments. (a) Nb versus $K_2O$ in hydrothermal–hydrogenous (HD–HT) sediments; turbidites and terrigenous clays (TB–TC) and sediments from various drill sites (all data from Vervoort et al., 2011). Many sediments have Nb/$K_2O$ ratios similar to average upper crust (R&G) and shales (PAAS, Nb from Barth et al., 2000), although individual sites possess distinct Nb/$K_2O$ ratios (e.g., ODP 701 South Sandwich terrigenous clays and DSDP 211 Nicobar turbidites). (b) Nb/Ta ratios in terrigenous clays (from ODP 1149, 701, 801, and 881, and DSDP 183, 495, and 321, from Plank et al., 2007; Vervoort et al., 2011); histogram gives average Nb/Ta = 14 ± 1 (1 standard deviation). Orange lines are average ± 1 standard deviation of individual sites, to illustrate regional variation in turbidites (DSDP 178 Alaska, DSDP 211 Nicobar/Java, and DSDP 174 Cascadia turbidites) and high values in hydrogenous clays (DSDP 596 Tonga), all from Vervoort et al. (2011). Bulk silicate earth (BSE) is from Munker et al. (2003); MUd from Queensland (MUQ) is from Kamber et al. (2005); and Murray–Darling Basin (MDB) sediments from Marx and Kamber (2010). Other upper crustal averages from Rudnick and Gao (see **Chapter 4.1**) and Barth et al. (2000). Chondrites range encompasses averages reported in Jochum et al. (2000) and Munker et al. (2003).

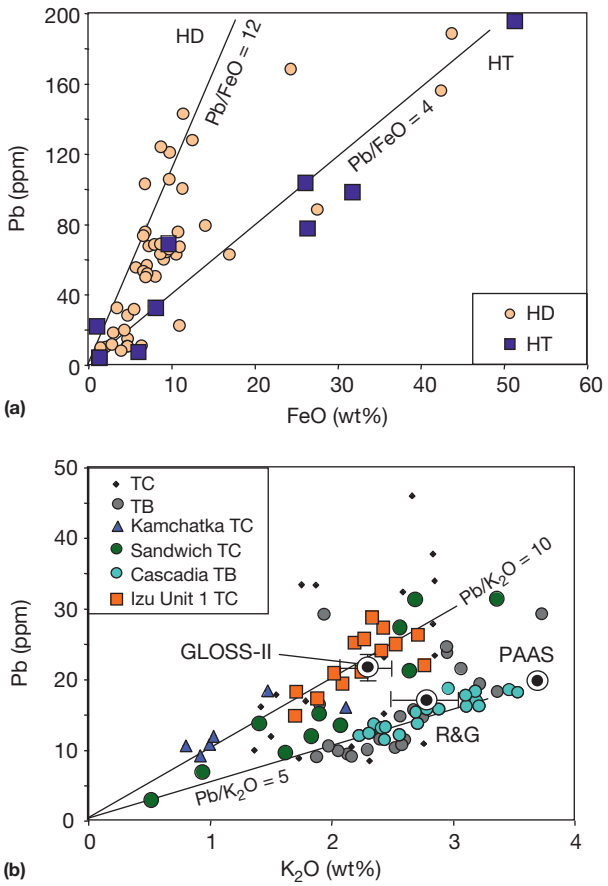


**Figure 5** Pb systematics in marine sediments. (a) Pb versus Fe in hydrogenous (HD) and hydrothermal (HT) sediments (designations and data in Vervoort et al., 2011). Hydrothermal sediments (within a few meters of basement) have a lower Pb/FeO ratio than hydrogenous sediment. (b) Pb versus $K_2O$ in terrigenous clays (TC) and turbidites (TB), with some drill sites identified. Turbidites generally have Pb/$K_2O$ ratios near those for upper continental crust (R&G) and average shales (PAAS), while some terrigenous clays have higher Pb/$K_2O$ (ODP 881 Kamchatka, ODP 701 South Sandwich, ODP 1149 Izu Unit 1 sediments, and DSDP 174 Cascadia turbidites highlighted), as does GLOSS-II. Data sources: Vervoort et al. (2011) and Plank et al. (2007).

and hydrogenous sediments, although the ratio is different between the two (**Figure 5(a)**). In hydrothermal sediments, the Pb/FeO ratio is around 4, as observed here and as in the classic study by Barrett et al. (1987) (with Pb/FeO = 4 ± 1). The ratio is closer to 10–20 in hydrogenous sediments, and some metalliferous crusts vary strongly with water depth, from Pb/FeO of >100 in 1000 m water to <20 at >3000 m (Aplin and Cronan, 1985). Sediments that subduct are generally deposited in deeper water, consistent with the lower end of this range (**Figure 5(a)**).

Remarkably, if sediments with significant hydrogenous and hydrothermal contributions are excluded, Pb has a predominantly detrital source and correlates strongly with $K_2O$ (**Figure 5(b)**). Most turbidites possess a ratio very similar to PAAS (Pb/$K_2O$ ~ 5–6) due to nearly quantitative delivery of continental material to the seafloor. Terrigenous clays generally have higher Pb/$K_2O$ ratios, with real differences between sites (e.g., Pb/$K_2O$ near six, upper crustal, for ODP 701 S. Sandwich Unit 1 diatom oozes, and Pb/$K_2O$ of ~10 for ODP 1149 Izu Unit 1 clays), possibly reflecting the variable effects of weathering on K and Pb.

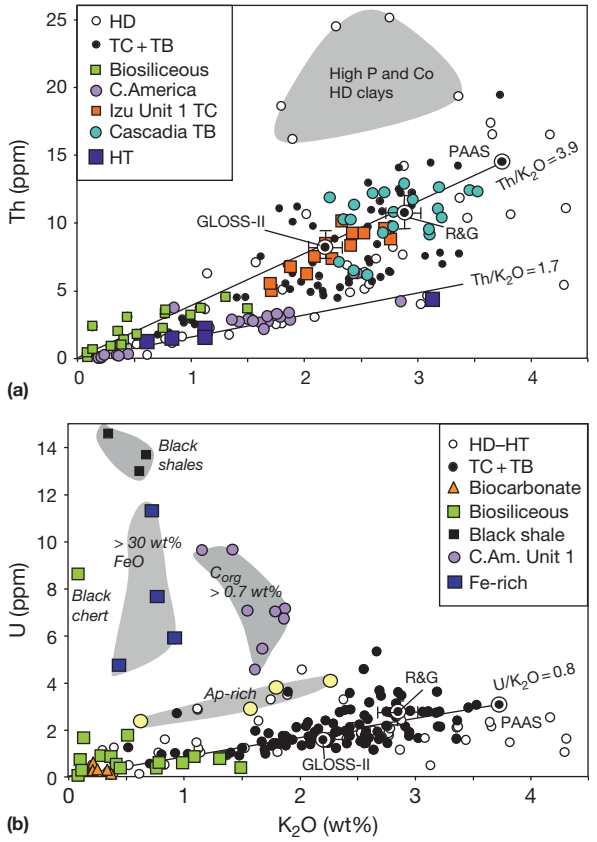


**Figure 6** Th and U in marine sediments. (a) Most marine sediments have $Th/K_2O$ ratios similar to those of average upper crust (R&G) and average shales (PAAS), with the exception of Th-enriched hydrogenous clays rich in phosphorus and cobalt. Hydrothermal sediments and ODP 844 Central American sediments have low $Th/K_2O$. (b) Most terrigenous clays and turbidites (TC + TB) and biogenic sediments have $U/K_2O$ ratios similar to those in average upper crust. Exceptions include U-enriched black shales, black chert, organic carbon-rich sediments from ODP 844 Unit 1 (Central America), apatite-rich sediments, and Fe-rich sediments. All data from Vervoort et al. (2011) and Plank et al. (2007).

#### 4.17.3.11 Thorium Revisited

The highest Th contents in marine sediments are found in phosphorus-rich (apatite-bearing fish debris) and Co-rich (low sedimentation rate) brown clays (Figure 6(a)). There is no indication of excess Th in hydrothermal sediments nor in many other hydrogenous sediments, and so there is no clear link to Fe or Mn oxides, as for Pb. Instead, the link to P and Co may reflect a similar process of seawater uptake in postmortem bioapatite, as for REE, where the greatest uptake occurs with greatest exposure to seawater (low sedimentation rate). Conodant apatite has been shown to take up Th, U, Pb, and REE in this manner (Trotter and Eggins, 2006). Nonetheless, with the exception of these unusual P-rich clays, most marine sediments possess $Th/K_2O$ ratios similar to UCC and PAAS (Figure 6(a)), ~3.5–4.0 (e.g., DSDP 174 Cascadia turbidites and ODP 1149 Izu Unit 1 clays) or lower (Central American sediments), likely reflecting some regional variation in continental and volcanic detritus delivered to the oceans.

#### 4.17.3.12 Uranium Revisited

U concentrations in marine sediments reflect many processes. The highest concentrations are found in black shales, in association with high levels of organic carbon, which drives authigenic U precipitation as $U^{IV}$. A striking example of this process is preserved in black shales of DSDP 144 Antilles sediments (Cretaceous Oceanic Anoxic Events 2 and 3; Carpentier et al., 2008) and Valanginian black chert in ODP 1149 Izu sediments (Chavagnac et al., 2008), both with extreme U enrichment (>8 ppm; Figure 6(b)) and extreme uranogenic Pb (i.e., high $^{206}Pb/^{204}Pb$). The hemipelagic sediments near the Central America trench are also unusually rich in organic carbon (up to 2 wt%; Summerhayes and Gilbert, 1982) and associated U (up to 10 ppm; Figure 6(b)), due largely to high biological productivity within the Costa Rica thermocline dome (Plank et al., 2002). In addition to organic carbon-rich sediments, Fe-rich (>30 wt% FeO), predominantly hydrothermal, sediments are also rich in U (>5 ppm). Like Th and REE, U is also taken up in postmortem bioapatite, for example, leading to excess U abundances in P-rich clays from DSDP 595/6 Tonga sediments. The remaining marine sediments, however, possess $U/K_2O$ similar to UCC and PAAS (0.8–1.0) or similar to their local detritus (Figure 6(b)).

### 4.17.4 Global Subducting Sediments

#### 4.17.4.1 Constructing GLOSS-II

The geochemical systematics in marine sediments may help not only in constraining UCC ratios (e.g., $Be/K_2O$) or whole earth ones (Nb/Ta) but also in making accurate estimates of the bulk sediments subducting at trenches and deriving a new global average, GLOSS-II. GLOSS has been a useful tool for geochemistry, but several factors motivate an update. First, of the 25 trenches considered in Plank and Langmuir (1998), 10 (Philippines, Ryukyu, Lesser Antilles, Cascadia, Alaska, Izu, Sumatra, Vanuatu, Central America, and Peru) have been newly sampled and analyzed for a wide suite of trace elements. Existing samples from six trenches (Tonga, Marianas, Kamchatka, Mexico, Aleutians, and South Sandwich) have been newly analyzed by ICP-MS for trace elements and isotopes. Two other margins, New Zealand and Chile, were not included in GLOSS, but new drilling, seismic surveys, and geochemical data enable their inclusion in GLOSS-II (which now includes 86% of the GLOSS mass flux). The new Li, Be, and B data, as well as the new systematics for key elements like Nb and Pb (Sections 4.17.3.6–4.17.3.12), have also motivated GLOSS-II. Details on data sources, averaging approaches, and site units are given in Appendix A, and new bulk compositions for each trench are given in Table 1, and GLOSS-II in Table 2. Reference drill sites for different trench segments are shown in the map in Figure 1, and a lithological summary is provided in Figure 7 (with a more detailed version in table form in the Supplement). The new data and interpretations discussed here have led to revisions in almost every trench sediment average.

The general approach in calculating the bulk sediment average for each trench is as in Plank and Langmuir (1998), where a small number (10–30) of representative geochemical analyses guide site estimates. This is possible because of the

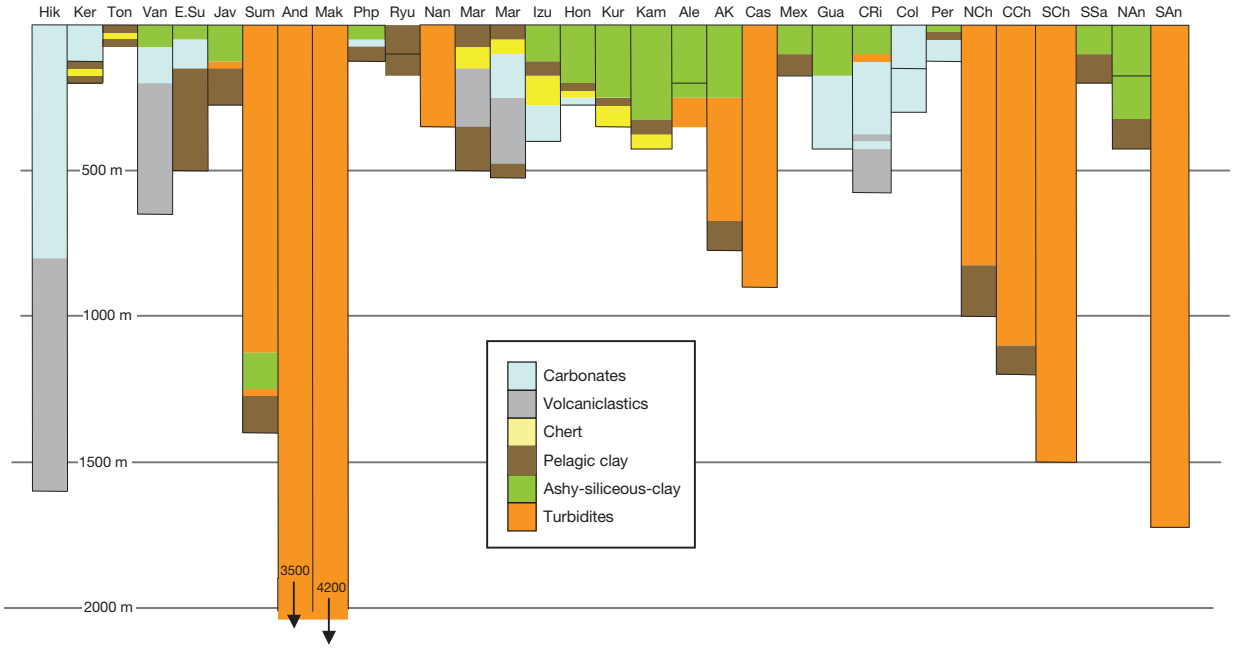


**Figure 7** Sedimentary thickness and summary lithology subducting at each trench. See supplementary Table B for a more detailed version of this figure, with site-specific lithological descriptions and reference drill sites.

wealth of data available for DSDP and ODP drill cores, including lithological information (e.g., estimates of biogenic material and turbidite layer thicknesses) and core index information (carbonate analyses, density, and water content). Downhole logging data can also be remarkably accurate, especially for K, U, and Th, which are commonly measured from gamma activity in the borehole after drilling. Plank et al. (2007) showed that these nearly continuous logging data yield unit averages that may agree within 5% (e.g., for Th) of discrete core analyses, supporting both the accuracy of the logs and the robustness of averages based on few samples ($n \sim 10$). Other studies have also estimated uncertainties in core averages of 20–30% (Carpentier et al., 2009; Plank and Ludden, 1992). The approach here takes advantage of the elemental systematics outlined above, specifically in the use of trace element ratios (e.g., $Pb/K_2O$), which may be consistent within individual lithological units and so used to estimate trace element concentrations from major element information. For example, shipboard $CaCO_3$ data can be used to calculate the mean CaO for a site (from stoichiometry) and then simple dilution relationships with elements like $K_2O$ can be used to derive mean $K_2O$ from mean CaO. Ratios of trace elements like Th or Nb to $K_2O$ can then be used to estimate site-averaged Th and Nb. Similar calculations can be carried out with natural gamma log K. The success of this approach is supported by the close similarity between GLOSS and GLOSS-II (see below).

These efforts have led to a dramatic improvement in the confidence levels for many trench sections (originally estimated by Plank and Langmuir (1998) from excellent, 1, to poor, 4). Eleven margins improved from confidence level 3–4 to 1–2. Some moved from 4 to 1 (Ryukyu, Izu, and Cascadia), while others that did not even exist in GLOSS (New Zealand and Chile) are now at confidence level 2. On the other hand, the greatest uncertainty in GLOSS still remains – the thickness and composition of the thickest sections, Andaman and Makran. These convergent margins flanking India involve subduction of the large Bengal and Indus fans and constitute ~40% of the mass of GLOSS-II. And yet little is known about the volume of material subducted, the lithological composition of undrilled deep sections, or the chemical composition of these sediments, aside from a handful of analyses. Some new data from DSDP Site 211, and for the sediments of the rivers and fans that feed these systems, have led to improvements in GLOSS-II. On the other hand, most thick sections are composed of terrigenous turbidites, similar in composition to average upper crust, and so this is unlikely to change the strong upper crustal contribution already in GLOSS.

### 4.17.4.2 Comparing GLOSS-II to GLOSS

For most elements, GLOSS-II varies from GLOSS by less than 10% (**Figure 8(a)**). This should provide some comfort to those who have used GLOSS to make various geochemical arguments over the years. This also supports the robustness of the method by which many elements were estimated in GLOSS. For example, Plank and Langmuir (1998) used the limited high-quality Nb data that existed at the time to demonstrate strong correlations with Ti and Al; this justified the use of Nb/Ti and Nb/Al ratios to estimate bulk Nb concentrations for many trenches with no actual Nb data. The estimates have proved to be remarkably accurate when compared to some here that are based on new ICP-MS analyses, within 5–10% for some trench averages (Mexico and Columbia) but more than 50% off for others (South Sandwich and Lesser Antilles). The agreement in Pb between GLOSS and GLOSS-II is also surprising given the lack of data that guided original guesses, which were based mostly on ratios to Th and REE.

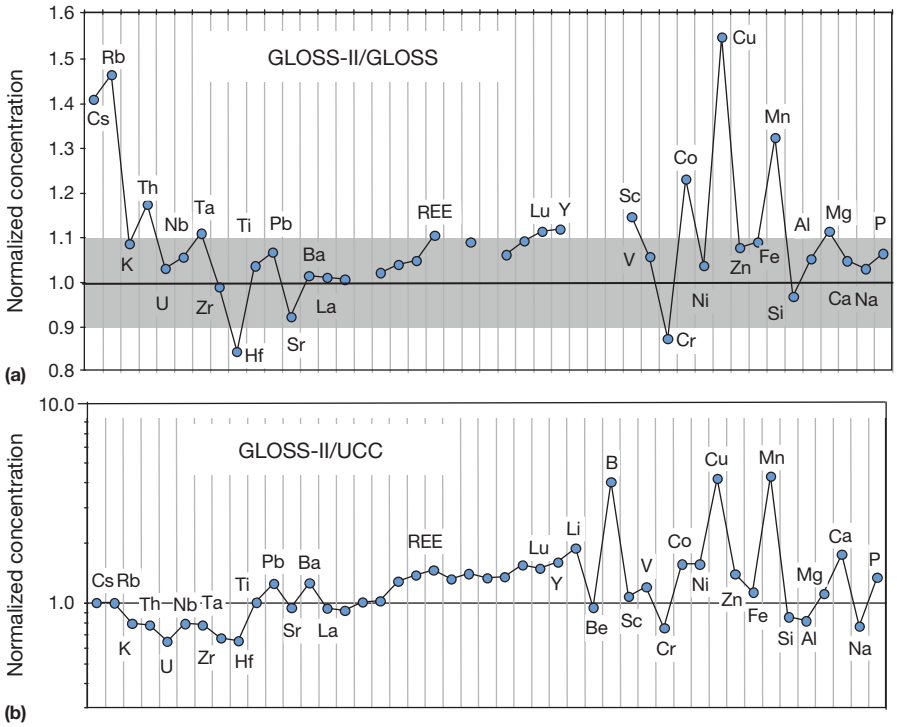


**Figure 8** Comparison of GLOSS-II to GLOSS and upper continental crust. (a) Concentrations in GLOSS-II (**Table 2**) normalized to original estimates for global subducting sediment (GLOSS) from Plank and Langmuir (1998). For most elements, GLOSS-II is within 10% of GLOSS (gray band). Some elements, notably Cu, Rb, Cs, Mn, Cr, Hf, and Th, reflect significant revisions. Gaps are for elements not included in GLOSS, but retained to keep the same ordering as in the panel below. (b) Concentrations in GLOSS-II normalized to the average upper crust estimate from Rudnick and Gao (see **Chapter 4.1**). Note log scale. See **Sections 4.17.4.2** and **4.17.4.3** for discussion of relative enrichments and depletions of GLOSS-II. Element ordering is as in Plank and Langmuir (1998) and reflects element groups (i.e., alkali elements, REE, and light elements).

GLOSS-II does differ significantly, however, from GLOSS for several important element tracers and ratios (Mn, Cu, Rb, Cs, Th, Hf, Rb/Sr, and Hf/Nd). For example, both Rb and Cs have increased by 40–50% in GLOSS-II (**Figure 8(a)**). While this derives from a significant increase in Rb and Cs in several trench sections (Andaman, Sumatra, Alaska, Cascadia, and Chile, which make up 44% of GLOSS-II by mass), by far the greatest effect derives from the Andaman section, which alone makes up 19% of GLOSS-II by mass. Its Rb increased by almost a factor of 3. This is because the previous estimate was based on no actual Rb data, guided by a single piston-core turbidite sample from McLennan et al. (1990), which has an anomalously low $Cs/K_2O$ ratio (and Rb was estimated from Cs). The new estimate is based on six new ICP-MS analyses of DSDP 211 Nicobar Fan turbidites. While six new analyses are still not a lot on which to hang the weight of Andaman sediment, they do define consistent $Cs/K_2O$ and $Rb/K_2O$ ratios. Coupled with small variation in the 13 samples that define a $K_2O$ average of $2.8 \pm 0.7$ wt%, the $Rb/K_2O$ ratio ($55 \pm 10$) yields average Rb ($144 \pm 46$ ppm) that never approaches the low Rb (24 ppm) of the previous estimate. Similarly, several of the other elemental differences (Th, Hf, and Cr) in GLOSS-II can be traced to the Andaman average. Thus, the new analyses at DSDP 211 that guide the Andaman and Sumatran sections are a significant improvement in GLOSS-II. These differences also lead to a large change in the Rb/Sr ratio (an increase of 60% in GLOSS-II), the parent/daughter ratio for the Sr isotope system. There is also a 20% increase in Nd/Hf, which may affect mixing relationships within the Hf–Nd isotope systems, and a 15% increase in Th/U.

### 4.17.4.3 Comparing GLOSS-II to UCC

GLOSS-II is also compared to average upper continent crust (see **Chapter 4.1**) in **Figure 8(b)**. As for GLOSS (Plank and Langmuir, 1998), the depletions and enrichments in GLOSS-II have to do with both marine processes and continental weathering. Some elements show hydrothermal–hydrogenous (Pb, Cu, Mn, and REE) and/or biogenic (Ca, P, and REE) enrichments in GLOSS-II relative to UCC. Others (e.g., K, Th, U, HFSE, and Cr) show depletion due to dilution of terrigenous material by biogenic phases (largely opal and carbonate). On the other hand, the enrichment in GLOSS-II of Rb, Cs, and Li relative to the other alkali element K is a weathering signal and reflects the predominance of continentally weathered material in marine sediments versus more juvenile constituents in UCC. The large B enrichment in GLOSS-II may be the largest weathering signal, given the lack of B enrichment in marine phases.

It is noteworthy how GLOSS (Plank and Langmuir, 1998) and GLOSS-II apparently record UCC ratios for many elements, in particular those not strongly fractionated in the oceanic realm by biological, hydrogenous, or hydrothermal processes (e.g., Zr/Hf, Ti/Al, Th/U, $Be/K_2O$, Nb/K, and Nb/Ta). This is perhaps unexpected, given that oceanic islands and island arcs also contribute significantly to the sediments on the seafloor, particularly seafloor that approaches trenches.

Nonetheless, such material apparently makes up a minor proportion of GLOSS, which is heavily weighted toward large submarine fans composed of continentally derived terrigenous sediments. This is consistent with the very similar $\varepsilon_{Nd}$ (CHUR) model age of GLOSS-II (1.0 Ga) and of the major river sediment and atmospheric dust average (1.1 Ga) reported in Goldstein et al. (1984), which is widely taken to reflect averaged UCC. The small shift in model age is consistent with slightly more juvenile material in GLOSS-II, which must largely consist of island arc material and not oceanic island material, given the low Ce/Pb ratio in GLOSS-II ($2.7 \pm 0.26$) and UCC ($3.7 \pm 0.5$) and many arcs (<3; Noll et al., 1996) versus the high ratio in oceanic basalts (20–30; Hofmann et al., 1986). If the shift in $\varepsilon_{Nd}$ from river sediments (−11.7; Goldstein et al., 1984) to GLOSS-II (−8.3) were entirely due to addition of juvenile arc Nd (with average $\varepsilon_{Nd}$ for Pacific arcs of +7.5; Jicha et al., 2004; Pearce et al., 1999; Tollstrup et al., 2010; Woodhead et al., 2001), then this would mean that ~17% of the Nd in GLOSS-II would be arc derived. Thus, GLOSS-II is predominantly composed of continental material and not juvenile arc or ocean island inputs.

The abundance of new ICP-MS Li data leads to a new estimate for Li in GLOSS-II of 45 ppm. This value is intermediate between that of UCC and PAAS, although the $Li/K_2O$ ratio of GLOSS-II (20) is identical to that of PAAS and more than double that of UCC (**Figure 2(a)** and **2(b)**). This supports a fundamental fractionation of Li and $K_2O$ during weathering of the continents, where clay-fraction sediments have higher $Li/K_2O$ than sands. Because much of GLOSS-II consists of sediment deposits at abyssal depths and far from continents, this fine-fraction material contributes to high $Li/K_2O$. Moreover, while there is wide variation in the $Li/K_2O$ ratio (from 10 to 30) both within and between different turbidite sections, the average ratio of turbidite samples here is close to 20. Thus, a $Li/K_2O$ ratio of 20, in PAAS and GLOSS-II, is a robust feature of marine sediments and shales but distinct from the UCC ratio (~9) due to fractionations that occur during continental weathering. The $Be/K_2O$ ratio of GLOSS-II (0.90) is nearly identical to that defined globally in terrigenous and biogenic marine sediments (0.86) and within the uncertainty of the UCC ($0.75 \pm 0.3$). The B/Li ratio of GLOSS-II (1.5) largely reflects the assumptions (B/Li = 1–2) that went into most trench sections, where B data are lacking.

The $\delta^7$Li composition of GLOSS-II ($+2.4 \pm 0.2$‰) is in accord with its CIA (54), which is not surprising given that the relationship in **Figure 2(c)** was used to estimate $\delta^7$Li in the many trench sections where no Li isotope data exist (for terrigenous sediments; other end-member $\delta^7$Li values were used to estimate biogenic and hydrogenetic sediments; see **Appendix A** for details). Nonetheless, the $\delta^7$Li of GLOSS-II is only slightly different from the global estimate in Chan et al. (2006), of +3‰, based on measurements from eight trench sections, representing 22% of the global mass flux of subducting sediments. GLOSS-II (at 86% of the global flux) is more representative, but major sedimentary sections (e.g., Andaman, Makran, and Chile) lack $\delta^7$Li measurements and rely on the CIA relationship. The scarcity of data notwithstanding, it is notable that both GLOSS-II and Chan et al.'s (2006) estimate of $\delta^7$Li in GLOSS are higher than PAAS, consistent with its greater CIA, and UCC, which is not (**Figure 2(c)**). The UCC appears to reflect highly weathered sources in its low $\delta^7$Li ($0 \pm 2$‰; Teng et al., 2004) but juvenile-granite type sources in its low CIA (51; **Chapter 4.1**), leading to it plotting well off the sedimentary array in **Figure 2(c)**. Whether this derives from a mismatch in the data suites that went into the compilations in Teng et al. (2004) and Rudnick and Gao (**Chapter 4.1**) or a real effect (S-type granites appear to have much lower $\delta^7$Li for a modest increase in CIA; Teng et al., 2004) awaits further study.

## 4.17.5 Implications for Recycling at Subduction Zones

While GLOSS estimates will always be heavily weighted to thick turbidite fans, with average upper crustal and shale compositions, the real value in calculating GLOSS-II is in the new geochemical information for each trench. For example, the new average chemical composition of New Zealand trench sediments only contributes 3% to GLOSS-II, and yet it represents a 100% improvement in the understanding of sediment subduction at New Zealand. Previous estimates were based solely on averaging a few surface piston cores (Gamble et al., 1996), which only sample the upper 10 m. The new estimate is based on drilling and analysis at ODP Sites 1123 and 1124 and new seismic reflection studies (Davy et al., 2008), which provide a more accurate basis for calculating the composition of the entire sedimentary column subducting at the Hikurangi margin of New Zealand. The new Kermadec sedimentary composition also includes turbidites derived from the Hikurangi Plateau, off New Zealand, and this has led to an improved match between the Kermadec sediment and the slab-mixing components to the arc (Todd et al., 2010). These are but two examples of the improvements in trench sediments estimates for subduction cycling problems.

A major utility of the trench averages that compose GLOSS-II is the tracing of elements through the subduction zone, from sediment input to arc volcanic output. Over the years, this endeavor has met with some success for certain tracers, for example, Pb isotopes (Woodhead, 1989), $^{10}$Be (Tera et al., 1986), B/Be (Morris et al., 1990), Ba/Na (Plank and Langmuir, 1993), Th/La (Plank, 2005), and Hf isotopes (Chauvel et al., 2009). Together, these isotopic and elemental tracers bear witness to the subduction recycling process. The challenge that remains is to use these input–output relationships to quantify the mass balance of recycling, to identify the mass-transfer processes in the subduction zone, and to constrain the pressure–temperature–$H_2O$ path of subducting slabs (see **Chapters 4.19**, **4.20** and **4.9**). Toward this end, it is important to recognize that each tracer may interrogate different parts of the system. For example, B may reflect low temperature fluid losses from the downgoing plate (Leeman, 1996; Marschall et al., 2007a), while REE and Th may reflect high temperature melt-like fluid losses (Hermann and Rubatto, 2009; Plank et al., 2009). Other tracers may be sensitive to a specific residual mineral, for example, Nb and Ta in rutile (Schmidt et al., 2004a; Turner et al., 1996) or K and Rb in micas (Hermann and Spandler, 2008; Tatsumi et al., 1991). Isotopic tracers like $^{207}$Pb/$^{204}$Pb and $^{176}$Hf/$^{177}$Hf potentially distinguish between

sedimentary and basaltic sources of fluids in the downgoing plate (e.g., Miller et al., 1994; Tollstrup et al., 2010). Understanding the full recycling process – amid the different dehydration reactions, residual mineralogy, and sources – requires a broad toolkit of tracers. Critical in this, then, are the multi-element constraints on sediment input at each trench, as provided here. Beyond GLOSS-II, this is the primary contribution of this chapter.

An exhaustive application of this compilation to arc recycling is beyond the scope of this chapter, and it is hoped that others will utilize the information here to pursue new questions related to the subducted contributions to arc magmas, and the lasting impacts on the continents and the mantle. However, given the new data for certain elements (Li, Be, and Nb), it is worth an initial glance at some sediment–arc relationships. As an example, the discussion below explores using Li/Y as a total flux monitor, Li isotopes to trace subducted sediment, $Be/K_2O$ to assess elemental fractionations, and Nb/La–Th/La to monitor the presence or absence of rutile. These examples are admittedly little more than teasers, and it is hoped that these preliminary observations spawn new work.

#### 4.17.5.1 Li/Y and Li Isotopes

There has been much interest in the cycling of Li through subduction zones, especially given the wide range in Li isotopic compositions of potential subduction inputs (e.g., sediments, altered oceanic crust, and serpentinite; Bouman et al., 2004; Chan et al., 1992, 2006; Marschall et al., 2007b; Vils et al., 2009) and potential fractionation during subduction metamorphism (Marschall et al., 2007b; Zack et al., 2003). Despite this promise, the Li isotopic composition of arc magmas in most cases overlaps with the range observed in MORB (Tomascak, 2004), possibly reflecting widescale re-equilibration with mantle wedge Li during melting and melt flow (Caciagli et al., 2011; Tomascak et al., 2002). Unlike many of the other arc tracers commonly examined (e.g., Pb, Th, and Ba), Li is a moderately incompatible element in mantle minerals (Brenan et al., 1998a, b; Caciagli et al., 2011; Ryan and Langmuir, 1987) and may exchange significantly during melting and mantle interaction.

While the isotopic signal is, in most cases, within the mantle noise, the elemental enrichment is ubiquitous. All arc magmas possess higher Li/Y ratios than MORB (0.2; Ryan and Langmuir, 1987), likely due to the release of Li and retention of Y in the slab. Indeed, laboratory experiments show a large fractionation between Li and Y (Johnson and Plank, 1999; Kessel et al., 2005; Klimm et al., 2008), with Y strongly partitioned into slab garnet and Li partitioned into slab fluids or melts that transport it to the sub-arc mantle melting region. On the other hand, Li and Y appear to have a similar bulk partitioning behavior in the mantle, even though their partition coefficients for individual minerals are different (Ryan and Langmuir, 1987). This explains the nearly invariant ratio in MORB and provides a useful background with which to quantify Li elemental enrichment in arcs. For example, lavas from the Antilles and Aleutian arcs have Li/Y ratios of around 0.4 (using data from Plank, 2005), roughly double that in MORB. These arc ratios likely have no bearing on the Li/Y ratio of the sediments subducting at those trenches (1.8–2.5) because of the large retention of Y in the slab. Instead, this could reflect a doubling of Li in the sub-arc versus sub-ridge mantle. If this is the case, then the Li/Y ratio might reflect the total amount of Li supplied by the subducting slab.

In order to test this notion, the Li/Y ratio is averaged for several arcs and plotted against the total Li flux entering the trench as marine sediments (calculated from **Table 1**). Indeed, there is a very strong correlation between the Li/Y of different arcs and the Li sediment flux entering trenches (**Figure 9**). Not only that, the y-intercept, at zero sediment flux, is the MORB value (0.2), presumably characteristic of the background mantle with no subducted inputs. The simplest way to interpret these observations is that the Li excess observed in arcs derives primarily from the subducted sediment. Where a greater flux of Li is delivered in marine sediments, the resulting arc volcanoes reflect a mantle source more enriched in Li. If altered oceanic crust and/or slab serpentinite also supplied excess Li, then the Li/Y intercept at zero sediment flux should be higher than the MORB value (as is observed for Sr/Na and Ba/Na; Plank and Langmuir, 1993). Instead, the MORB Li/Y intercept is consistent with mantle–sediment mixing alone. If this interpretation is correct, then Li/Y is a high fidelity monitor of total Li sediment flux. This view contrasts with the 'attenuated' Li signal emphasized by Tomascak et al. (2002), Caciagli et al. (2011), and Halama et al. (2009). This may be the view from the isotopes, but the trace element enrichment is strong and potentially strongly linked to sedimentary Li.

Several aspects of the Li/Y data bear further scrutiny, however. The arc data point with the highest Li/Y is South Chile, and yet this is represented by only five analyses (of mafic enclaves $<55\%$ $SiO_2$) from a single volcano (Nevado de Longavi), which is somewhat anomalous in its geochemical behavior (Rodriguez et al., 2007). Nonetheless, it is the only volcano from the southern volcanic zone of Chile that has any Li data published and reported in Georoc (including over 1000 analyses). Clearly, more Li data are needed for mafic volcanic rocks of the Chilean arc. Moreover, the high-Li sediment flux at the Chile trench is largely a function of the great thickness ($\sim$1 km) estimated to fill the subduction channel (Contreras-Reyes et al., 2010), and there is significant uncertainty in how much of that sediment subducts to depth. Nonetheless, removal of the South Chile datum only decreases $R^2$ from 0.97 to 0.88, so the rest of the correlation is still highly significant. There is also an increase in Li/Y from island arcs (like Tonga and the Marianas) to continental arcs (like the Cascades and Chile), although again, $R^2$ (0.88) for just the island arcs (excluding the Cascades and Chile) is still highly significant. Y is strongly compatible in garnet, and so it is possible to fractionate Li/Y with mantle or crust processes involving garnet. Yet, all the arcs examined form steep vertical trends in Li/Y versus Dy/Yb plots, unlike OIBs which clearly involve garnet in their melting source (see Ryan and Langmuir, 1987). Moreover, the magmas with the lowest Y content (Tonga) have the lowest Li/Y, not highest, and so Y variations are not dominant. In fact, the full range of arc Li/Y ratios is expressed at typical Y concentrations of 15–20 ppm. There is still a dearth of quality Li concentration data on mafic arc volcanic rocks (due largely to the widespread use of lithium fluxes in sample preparation), and the preliminary correlation in **Figure 9** should motivate further work.

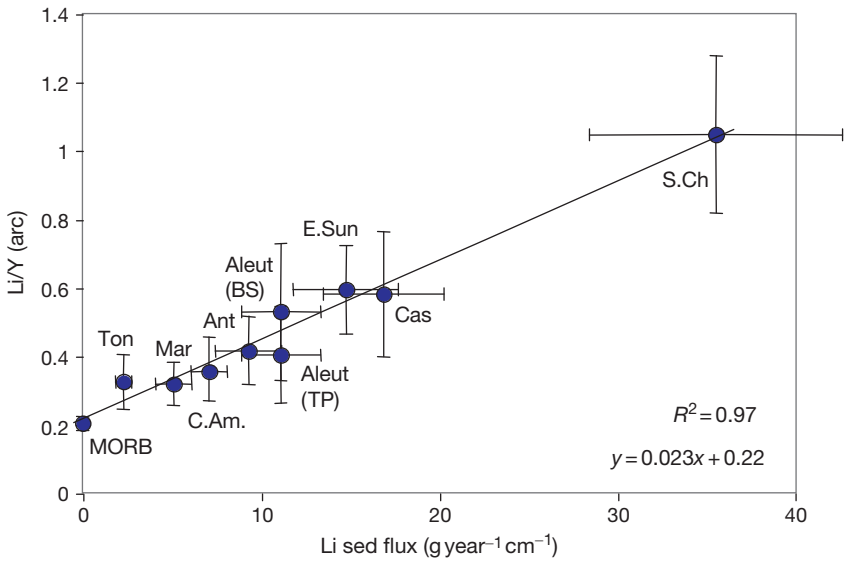


**Figure 9** Correlation between Li sediment flux and Li/Y in arc magmas. Line is linear regression, which intersects the origin near the MORB Li/Y value (0.2; Ryan and Langmuir, 1987). Li sediment flux is calculated from concentrations and mass fluxes given in **Table 1** for different trenches; error bars include 20% uncertainty. Volcanic data are averaged for most mafic samples (generally <55 wt% $SiO_2$) from each arc; error bars reflect one standard deviation. Data sources: Tonga arc (Cooper, 2009; submarine volcanoes 1 thru L); Marianas arc (unpublished ICP-MS data, Plank and Wade); Antilles arc (Plank, 2005); Aleutians BS (B. Singer et al., 2007); Aleutians TP (Plank, 2005); E. Sunda (unpublished ICP-MS data, Turner and Plank); the Cascades (Leeman et al., 2004; Prueher and McBirney, 1988; Magna et al., 2006; and unpublished ICP-MS analyses, Grove and Plank); South Chile (Rodriguez et al., 2007; including mafic enclaves); and Central America (Centam database, Carr et al., 2007, including unpublished ICP-MS data, Plank and Carr).

The sedimentary Li/Y correlation also has implications for Li isotopic variations in arcs. If the Li enrichment in arc magmas derives primarily from the sedimentary Li flux, then why are the isotopic variations so limited and overlapping with MORB? The community view on this is that Li is isotopically equilibrated with the mantle (Halama et al., 2009; Tomascak et al., 2002) due to its significant solid/fluid partitioning into mantle minerals (e.g., Brenan et al., 1998a; Caciagli et al., 2011) and its high diffusivity (e.g., Dohmen et al., 2010). There are several problems with this view, however, as recently demonstrated by Caciagli et al. (2011). If Li were extensively equilibrated with the mantle in a chromatographic column-type process, then so too would be Y, since both elements have similar bulk partition coefficients. Likewise, diffusive equilibration of Li will only reduce the Li/Y of the melt, driving it toward MORB values. The Li isotopic composition of arc magmas might also then be much heavier than observed (as modeled by Caciagli et al., 2011), and so both the elemental and isotopic observations are difficult to reconcile with such an efficient reactive transport process. The high Li/Y of arc magmas is a strong constraint on the extent of equilibration of Li between melt and mantle. Another way to interpret the MORB-like $\delta^7$Li of many arc basalts is to recognize that the bulk Li isotopic composition of many marine sedimentary sections does not actually vary greatly outside the MORB range, so there is little leverage in most mixing scenarios that involve sedimentary Li. For example, the $\delta^7$Li of GLOSS-II is $+2.42 \pm 0.18$, within the range of MORB.

Nonetheless, some sedimentary sections have more extreme $\delta^7$Li: Marianas and Tonga bulk sediment (+9 and +7‰, respectively), which is heavy because it is dominated by marine authigenic and biogenic phases, and E. Sunda and Lesser Antilles bulk sediment (+0.3 and −0.4‰, respectively), which is light because it is dominated by terrigenous phases (Bouman et al., 2004; Chan et al., 2006). Unfortunately, there is generally insufficient published arc data to test these mixing relationships here. The exception is E. Sunda (Tomascak et al., 2002), where nine samples from three volcanoes on Lombok show a rough correlation in $\delta^7$Li and Y/Li (inverted here to vary linearly with $\delta^7$Li), consistent with mixing between mantle Li ($\delta^7$Li ~ +5‰) and lighter slab Li (**Figure 10(a)**). For some samples, the slab end-member is well fit by the isotopic composition of the bulk sediment (based on DSDP 262 data measured by Bouman et al., 2004 and averaged by Chan et al., 2006). For others, a heavier isotopic composition is a better match. A 3‰ shift to heavier fluid compositions is consistent with the isotopic fractionation factor at high temperatures (>500 °C for clinopyroxene; Wunder et al., 2006). However, Marschall et al. (2007b) demonstrate how the solid may shift to lower $\delta^7$Li during incremental dehydration but that the shift is unlikely to be more than −3‰. If the solid shifts down by 3‰ and the fractionation factor between fluid and solid is +3‰, it is possible that the Li isotopic composition of high-temperature fluid that exits the slab and transports Li to the mantle wedge is very similar to that of the initial bulk solid. Lower temperature metamorphic dehydration reactions (subgreenschist to greenschist) are expected to have little effect on the Li isotopic compositions of the subducting assemblage; despite the greater fractionation factor at low temperature, the partition coefficients for Li are very large (>1; Marschall et al., 2007a), and so there is little expected loss of Li to fluid at low temperatures with which to affect the isotopic composition of the solid (Marschall et al., 2007b). This lack of Li isotopic variation is also borne out in

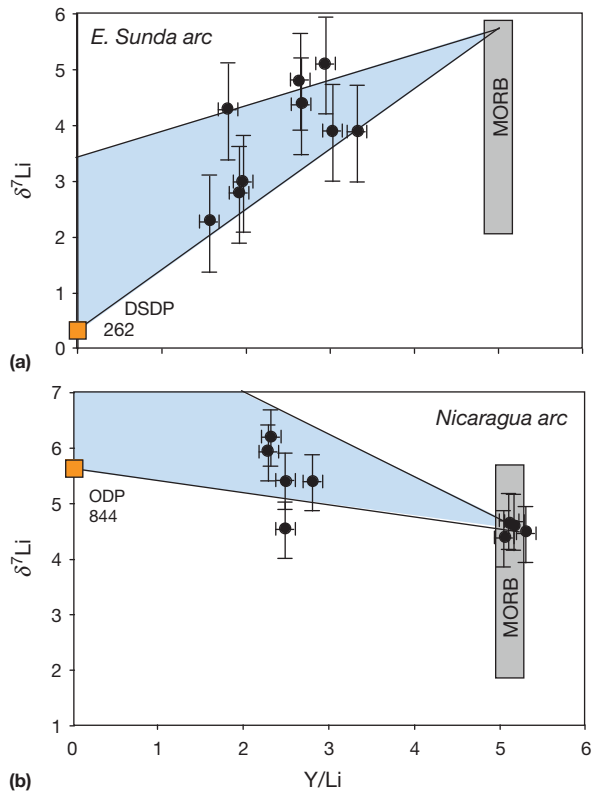


**Figure 10** Li isotope systematics in (a) E. Sunda and (b) Nicaragua arc. Both arc datasets (black circles) show correlated variation between $\delta^7$Li and Y/Li, consistent with mixing between mantle in the MORB field and local sediment. Y/Li is the inverse of elemental Li enrichment (as in Li/Y in **Figure 7**) and is plotted this way so that mixing is a straight line. With decreasing Y/Li, the E. Sunda arc mixes toward lower $\delta^7$Li than its inferred MORB source, consistent with the low $\delta^7$Li of the terrigenous sediments of DSDP 262. Nicaragua arc mixes from the MORB field to higher $\delta^7$Li as Y/Li decreases, consistent with the higher $\delta^7$Li of the ODP 844 carbonate and hemipelagic oozes. The orange boxes are the bulk sediment estimates from Chan et al. (2006). Blue triangles show mixing scenarios for fluids with bulk sediment Li and up to 3‰ heavier, consistent with fluid–solid fractionation that may occur during high temperature dehydration of sediment (see text, and Marschall et al., 2007b). E. Sunda arc data from Tomascak et al. (2002) with error bars of ±1‰ for isotopes and ±0.1 for Y/Li; Nicaragua data from Chan et al. (2002) with error bars of ±0.5‰ for isotopes and ±0.1 for Y/Li.

field studies of mudrocks at low metamorphic grades (Qiu et al., 2009, 2011) and of metapelite in contact aureoles (Teng et al., 2007). Thus, given the limited fractionation of Li isotopes that may occur at high temperature (with the caveat that fractionation factors are unknown for most of the relevant phases), arcs might mix toward slab $\delta^7$Li that is similar to or up to 3‰ heavier than the bulk sediment composition. This is illustrated in **Figure 10(a)** and is broadly consistent with the E. Sunda arc data.

The Nicaragua sector of the Central American arc (nine samples from five volcanoes) also shows a correlated variation between Y/Li and $\delta^7$Li (Chan et al., 2002), consistent with mixing between MORB mantle and slab Li with the isotopic composition (and up to 3‰ heavier) of the bulk ODP 844 sediment (**Figure 10(b)**), as estimated by Chan et al. (2006). The Izu arc (six samples from six volcanoes) also shows correlated variation between Y/Li and $\delta^7$Li (Moriguti and Nakamura, 1998), but no analyses exist of ODP 1149 sediments subducting there. The arc values require mixing with very heavy $\delta^7$Li (+18) which is consistent with some radiolarian cherts (Marianas radiolarites in Bouman et al., 2004) or low temperature fluids from altered oceanic crust (Marschall et al., 2007b). Clearly, the Li isotopic data are as yet sparse, but targeted studies of arc basalt Li isotopes, in samples that show a range in Li/Y, and from regions where distinctive sedimentary Li isotopes subduct, may further test the sediment source versus mantle reequilibration mechanisms.

### 4.17.5.2 Be/$K_2O$

Be is an important tracer in the subduction zone because of its short-lived cosmogenic nuclide, $^{10}$Be. $^{10}$Be is formed in the atmosphere, stored in sediments for ~10 My, and found in anomalously high abundances in arc magmas, relative to those from other tectonic settings (Tera et al., 1986). The remarkable interpretation for these observations is that the uppermost marine sediments (<10 Ma), which contain $^{10}$Be, are subducted to the depths of arc magmagenesis (~100 km), where $^{10}$Be is extracted from the slab during dehydration or melting reactions, then rapidly recycled to the surface via arc magmas. Despite this 'smoking gun' evidence for rapid and efficient sediment recycling at subduction zones, the behavior of Be during subduction is still not well understood. What are the important mineral carriers? How much is lost in the first 100 km? What reactions give up Be to slab fluids/melts? Marschall et al. (2007a) consider Be loss during subduction of mafic assemblages and conclude that it is nearly quantitatively retained in solid phases up to 700 °C. The losses from marine sediments, however, are less well understood, in part due to the wide range in bulk compositions.

The roughly constant Be/$K_2O$ ratio in most marine sediments (0.86 ± 0.04, **Figure 2(d)**; and 0.9 in GLOSS-II, **Table 2**) provides a potentially useful tool in exploring the behavior of Be in subduction zones. If bulk sediment contributes to the arc magma source, or if Be and K behave similarly to one another during mass transfer from the slab, then arc magmas should mix toward the sediment Be/$K_2O$ ratio near 0.9. In order to test this, four arc magma suites with high-quality ICP-MS Be data are plotted in **Figure 11(a)**, as Be/$K_2O$ versus Nb/$K_2O$. The rationale behind the use of the Nb/$K_2O$ ratio is that slab fluids are thought to have very low Nb/$K_2O$ (approaching zero if Nb is largely retained in the subducting slab) while mantle melts (MORB) have high ratios (generally >20; Niu and Batiza, 1997), and so this helps to elucidate the slab fluid–mantle mixing relationships that contribute to the final arc product. The Be/$K_2O$ ratio in the arc basalts generally varies from a low value in the slab end-member (≤1) toward a higher value, typical of MORB (>3). Each arc suite can then be unmixed, with the Be/$K_2O$ intercept at zero Nb/$K_2O$ taken to be the inferred Be/$K_2O$ of the slab fluid/melt end-member. These intercepts (Be/$K_2O$ = 0.4 – 1.2) are generally near the compositions of bulk sediments (0.9) but in detail, vary significantly in each region. Tonga shows the greatest fractionation, where the bulk sediments at the trench have a Be/$K_2O$ ratio of 0.84, while the arc data clearly project to much lower ratio (0.4, which

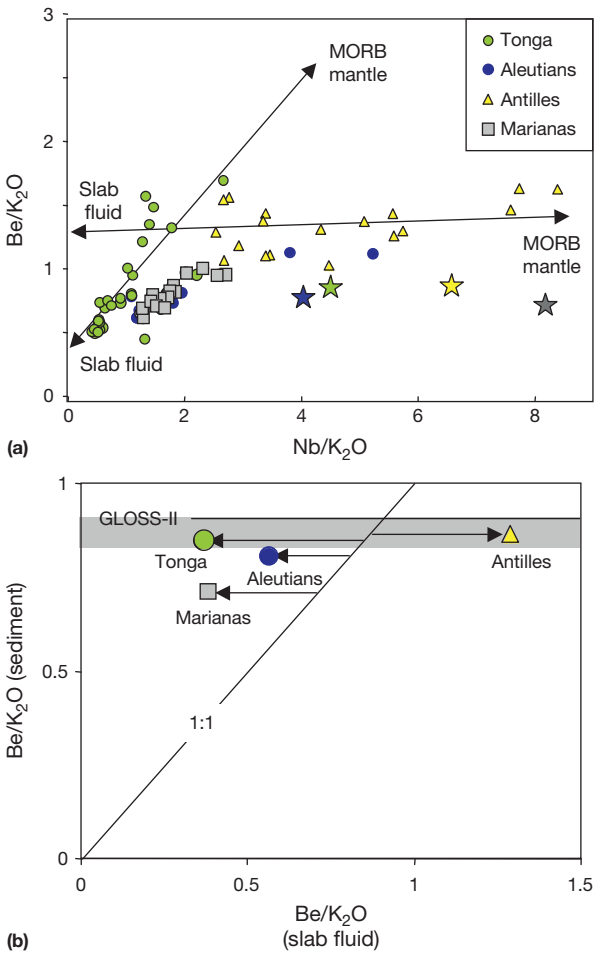


**Figure 11** $Be/K_2O$ systematics in arcs. (a) $Be/K_2O$ versus $Nb/K_2O$. Arcs arrays can be unmixed (by linear regression) on this diagram to reveal slab fluid end-member, with assumed zero $Nb/K_2O$, as illustrated for the Antilles and Tonga arcs. Stars are bulk sediment estimates at the trench (**Table 1**), color coded to the relevant arc. (b) The $Be/K_2O$ ratio of the projected slab fluid (from (a)) plotted against the $Be/K_2O$ ratio of the bulk sediment at each trench (**Table 1**). Arcs do not fall on the 1:1 line and plot at both lower and higher $Be/K_2O$ than bulk sediment, demonstrating variable fractionation of Be and $K_2O$ in the subduction zone. Arc data sources as in **Figure 8**.

would be so even without projecting to zero $Nb/K_2O$), implying a factor of 2 fractionation between Be and K in the subduction zone. On the other hand, the Antilles arc data have a fairly uniform $Be/K_2O$ ratio, between 1 and 1.5, which is higher than the $Be/K_2O$ ratio of 0.86 found in most terrigenous sediments (**Figure 1(d)**). Note that there are no actual Be measurements in Antilles trench sediment (Carpentier et al., 2009), and so the average in **Table 1** and **Figure 11** is taken as 0.86. New analyses would test whether unusually high ratios exist in the Antilles sediment input. Even with this uncertainty, however, the sense of fractionation between the Antilles and Tonga is completely different and the basic observation is that arcs mix to slab fluids that vary considerably more in $Be/K_2O$ than sediment input (**Figure 11(b)**).

This fractionation in $Be/K_2O$ signals different behavior of Be and K in different subduction zones, possibly due to differences in slab temperatures (Plank et al., 2009). Certainly, the Tonga and Lesser Antilles arcs are end-members in convergence velocity, as well as in sediment thicknesses. Unfortunately, few laboratory experiments on sediment dehydration/melting include both Be and $K_2O$ in the starting composition. Notably, several experimental studies have constrained well the behavior of K and micas, but do not include Be (Hermann and Spandler, 2008; Schmidt et al., 2004b; Skora and Blundy, 2010). On the other hand, the experiments of Kessel et al. (2005) include Be and show a clear increase in its partitioning into fluids with increasing temperature, but unfortunately, the experiments were K-free. The only experimental study that includes both Be and K is that of Johnson and Plank (1999), which does predict variations in $Be/K_2O$ with temperature. At low T, below the solidus, Be behaves more compatibly in solids than K, and so fluids have low $Be/K_2O$. Above the solidus, Be becomes mobile while K remains strongly compatible in mica, and so melts have high $Be/K_2O$. This is the same sense as the variations observed in Tonga (below the solidus, low $Be/K_2O$) and Antilles (above the solidus, high $Be/K_2O$). Given the rich mineral assemblages, it is difficult to predict exactly why such a change in ratio would occur, but it may have to do with the likelihood of Be being less compatible in phengite than K, generating high $Be/K_2O$ sediment melts just above the solidus. Alternatively, low $Be/K_2O$ may originate in the mafic portions of the slab, where temperatures may be lower than the sediments at the slab surface and the mode of phengite lower due to the lower K abundances. In this case, Be may be more compatible than K due to its higher compatibility in other silicates, such as pyroxenes and amphiboles in which Marschall et al. (2007a) predict min/fluid $D$'s $>1$. The nearly constant sediment $Be/K_2O$ ratio, with large variations in arc magmas, motivates further work in the laboratory to determine if $Be/K_2O$ has potential as a thermometer or tracer of sediment versus basalt contributions.

### 4.17.5.3 Nb/La and Th/La

Unlike Li/Y, which may reflect bulk Li sediment flux, and $Be/K_2O$, which may be fractionated in the subduction zone, some element ratios appear to faithfully transfer from the subducting sediment to the arc. The clearest example of this is Th/La, which was explored in detail in Plank (2005). The bulk sediments subducting at different trenches worldwide vary by about a factor of 5 in their Th/La ratio, from $<0.1$ in hydrogenetic clays rich in biophosphates to $>0.35$ in terrigenous sediments, reflecting the upper crustal ratio ($0.33 \pm 0.05$, as compiled in Plank, 2005). These same variations are recorded in the local arc volcanic rocks, which form mixing trends that typically project to high Th/La end-members that are very similar to the bulk sediment at the trench. **Figure 12(a)** illustrates the utility of Th/La, by plotting it against Sm/La, so that mixing between mantle and sediment is a straight line. Mafic magmas from a given arc (the Marianas and South Sandwich are illustrated, for example) form linear arrays that may be unmixed to reveal their end-members on the MORB array at one end and something very similar or identical to the bulk subducting sediment at the other. In the example shown, the South Sandwich arc data project to much higher Th/La than the Marianas arc data, reflecting the terrigenous

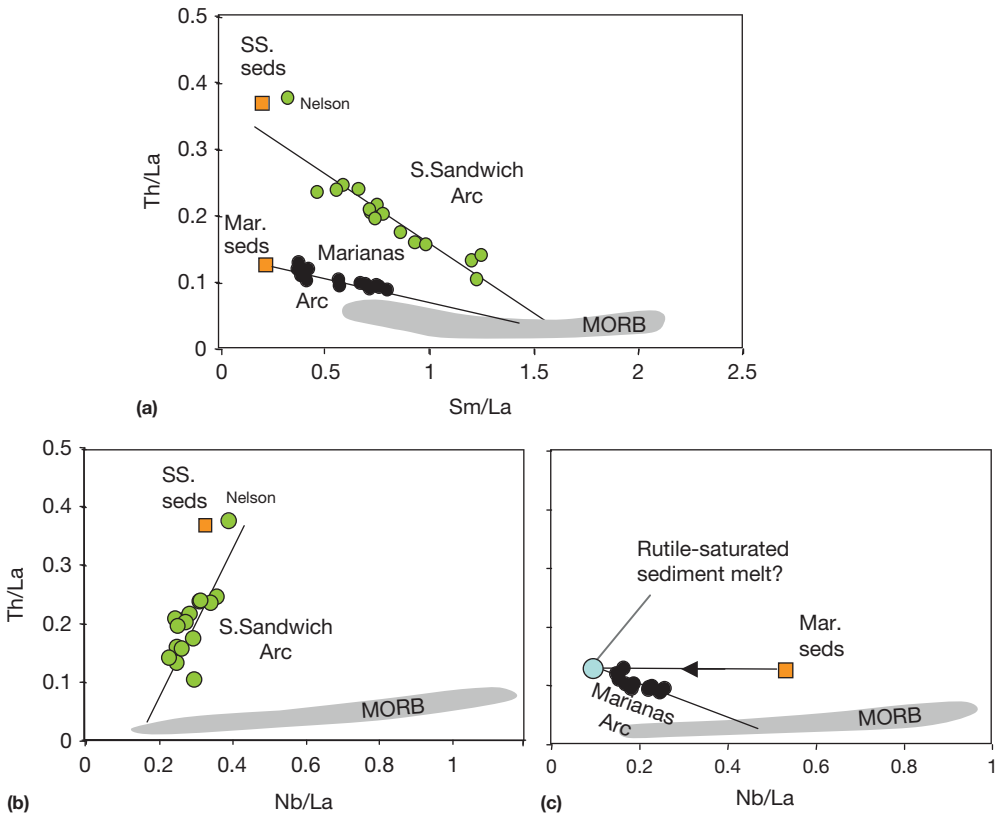


**Figure 12** Th/La–Nb/La systematics in arcs. (a) Th/La versus Sm/La, as in Plank (2005), for Marianas and South Sandwich arcs. Arcs generally form arrays that can be unmixed linearly to an end-member in the MORB array and a high Th/La end-member that is typically very similar to bulk sediment (orange boxes, **Table 1**), demonstrating little fractionation of Th from La in subducting sediments. Th/La versus Nb/La for (b) South Sandwich arc and (c) Marianas arc illustrate contrasting behavior of Nb. The South Sandwich arc mixes between MORB and a component with Nb/La similar to (or higher than) its bulk sediment, whereas the Marianas arc data require a sedimentary component with greatly reduced Nb/La, consistent with rutile-saturated melting. Data sources: Marianas arc data (<53% $SiO_2$) from Elliott et al. (1997). South Sandwich arc data are from multiple studies (Barry et al., 2006; Pearce et al., 1995; Plank, 2005) and individual data points show some scatter. Thus arc averages are plotted here to illustrate arc-wide trends. MORB array from Niu and Batiza (1997). Nelson seamount samples have been interpreted to reflect sediment melt end-member (Leat et al., 2004). Lines through arc arrays are linear regressions.

clays subducting at the South Sandwich trench, which have Th/La very similar to UCC. These mixing relationships are observed for most arc data acquired by high-quality ICP-MS analysis (Plank, 2005), and the sediment end-member is almost always very similar to the bulk sediment. There is thus little evidence for fractionation of Th from La in the subduction zone, which makes this trace element ratio behave much like an isotope ratio (e.g., $^{143}Nd/^{144}Nd$), yet with a much bigger dynamic range (fivefold). The lack of Th/La fractionation from bulk sediment values also constrains possible residual minerals that may exist in the subducting slab (Skora and Blundy, 2010). Regardless of how the ratio is preserved, Th/La provides a simple reference with which to observe the behavior of other important subduction tracers.

For example, in addition to high Th/La, most arc basalts also possess low Nb/La (and, obviously, very high Th/Nb). These are common geochemical fingerprints of arcs, usually illustrated as spikes and troughs in spider diagrams (see **Chapter 4.21**, and references therein). High Th/La and low Nb/La are also inherent features of marine sediments, and the discussion above demonstrates how arcs may simply inherit the high Th/La ratio of sediments. How much of the low Nb/La (i.e., the 'Nb anomaly') is inherited from marine sediments? To explore this, Th/La is plotted against Nb/La for the same Mariana and South Sandwich arc data in **Figure 12(a)**. Again, the South Sandwich arc could be consistent with bulk mixing of the local subducting sediment and a highly depleted mantle (**Figure 12(b)**; the regressed line actually projects to higher Nb/La, but bulk sediment is also permissible). This is especially apparent considering the Nelson seamount samples, which have been interpreted based on their Nd isotopes and other characteristics (like their high Th/La) to be consistent with a strong recycled sediment component (Barry et al., 2006; Leat et al., 2004). If this is the case, then at least for some arcs, there is no need to fractionate Nb significantly from the other trace elements and the arc simply inherits the sediment's Nb anomaly (largely due to the high Th/Nb). This also means that Nb is not 'conserved' in all subduction zones (Pearce et al., 2005) but that even in the South Sandwich arc, where magmas are demonstrably depleted in Nb concentration, there is still transfer of Nb from the slab to the mantle. Other arcs that are also consistent with simple recycling of the Nb anomaly and show little net fractionation of Nb from REE and Th include Tonga, Izu, Honshu, and Vanuatu (data and references as in Plank, 2005).

On the other hand, the Marianas arc requires a very different end-member from the sediment subducting at the trench (**Figure 12(c)**), one with much lower Nb/La (by approximately a factor of 5). The Nb depletion is strongly correlated with increasing Th/La and so likely also derives from the sediment, albeit one with a very low Nb/La. Such inferences about Nb fractionation are also apparent from other trace element and isotopic considerations (Elliott et al., 1997). Strong fractionation of Nb from La and Th is generally thought to require residual rutile in the subducting slab, a mineral that strongly partitions Nb and Ta (with $D$(xl/fluid ~10–100); Klimm et al., 2008; Schmidt et al., 2004a). This kind of behavior is also observed for other arcs, such as the Aleutians, in Nb/Th–$^{143}$Nd/$^{144}$Nd mixing relationships (Class et al., 2000). These arcs inspire the common notion that Nb is largely 'held back' and 'conserved' in subducting assemblages and that the Nb anomaly observed in arcs is generated, or accentuated, in the subduction zone. Other arcs that appear to require Nb fractionation include the Cascades and the Lesser Antilles (Carpentier et al., 2009; Grove et al., 2002; Turner et al., 1996).

Thus, some arcs largely inherit the sediment's Nb anomaly, while others reflect its active generation in the subduction zone. Why do different subduction zones exhibit different behavior? One possibility is that rutile is not a ubiquitous residual mineral in subducting sediments, and that, depending on bulk compositional parameters (Ti/Fe and $Fe^{3+}/Fe_T$), other oxides may predominate (magnetite and ilmenite). Indeed, in the $Fe^{3+}$-rich, low-Ti/Fe Tonga red-clay composition studied by Johnson and Plank (1999), rutile was identified in only one experiment (at 4 GPa and 1000 °C), with magnetite and ilmenite as the dominant Fe–Ti phases in most experiments. As such, Nb was not fractionated significantly from the REE, and there was no new Nb anomaly generated in these experiments. This contrasts with the experiments of Hermann and Rubatto (2009), where rutile grew ubiquitously in a GLOSS-type starting composition (at the nickel–nickel oxide $fO_2$ buffer, NNO), as did the experiments of Skora and Blundy (2010) on Antilles radiolarian clay (also at the NNO). Thus, the behavior of Nb with respect to sediment melting may vary from arc to arc depending on the major element composition of the sediments.

It is no wonder, then, that the Nb anomaly has been one of the most complex observations to explain in arcs. It likely depends on at least three independent factors: (1) the composition of the background mantle (which may vary by more than a factor of 5 in Nb/La; **Figure 12(b)** and **12(c)** and Hawkesworth et al., 1993), (2) the composition of the local sediment (where Nb/La varies by a factor of >5 in the input; **Table 1**), and (3) variable fractionation in the subduction zone caused by the presence or absence of rutile. Further work is warranted in both the experimental laboratory (to explore the conditions under which rutile forms, as well as the effect of anion solution complexes) and the analytical one (to determine the Nb anomaly in arc basalts with high-quality ICP-MS measurements in samples that have not been contaminated during powdering in tungsten carbide). Another prerequisite to resolving the different competing processes is to constrain well the initial Nb anomaly within the sediments subducting at the trench, as provided here.

### 4.17.6 Future Prospects

The sedimentary compositions at deep-sea trenches will continue to bring insight into marine, continental, and subduction processes. The dramatic increase in high-quality, multi-element ICP-MS data has warranted a fresh look at each trench and a recompilation of GLOSS-II. This has resulted in substantial revision to many trench compositions, significant revision to GLOSS, and new estimates for some trenches (New Zealand and Chile) and some elements (Li, Be, and B).

While trench sediments are now fairly well characterized for many major and trace elements, future work will need to focus on important radiogenic isotope systems (Hf) and a growing list of stable isotope systems (O, Li, B, S, Cl, Mg, V, Tl, and Fe). A major gap in characterizing subducting budgets, however, is in volatile species. $H_2O$ and inorganic carbonate are fairly well characterized in the trenches that make up GLOSS-II, but S, Cl, N, and organic C and their isotopes are clearly critical to important earth cycles, and comprehensive data and/or compilations do not currently exist. These analytes represent clear targets for future work, as do continued efforts to model the downstream effects of subducting sediment on volcanic arcs, the continents, and the mantle.

## Acknowledgments

Thanks to Roberta Rudnick for encouraging the writing of this chapter and for her helpful comments and careful editing. The author owes a special thanks to Charlie Langmuir for the initial inspiration to work on sediment subduction years ago. This effort would not have been worth doing without the new data collected with Jeff Vervoort. Many colleagues have provided inspiring thoughts on the topic of subduction recycling, including Tim Elliott, Catherine Chauvel, Simon Turner, Jim Gill, Bill White, Peter Kelemen, Horst Marschall, and Julie Prytulak. The author especially thanks Donna Shillington, Horst Marschall, and Tim Elliott for some speedy help. The author is grateful to the Lamont-Doherty Earth Observatory and Columbia University for the freedom to work on a project like this for a semester and to the National Science Foundation and Boston University for support of the ICP-MS trace element data collection (OCE-0137110, EAR-0549641, OCE-0839061, EAR-0852462).

## References

Aplin AC and Cronan DS (1985) Ferromanganese oxide deposits from the Central Pacific Ocean, I. Encrustations from the Line Islands Archipelago. *Geochimica et Cosmochimica Acta* 49: 427–436.

Barrett TJ, Taylor PN, and Lugowski J (1987) Metalliferous sediments from DSDP Leg 92: The East Pacific Rise transect. *Geochimica et Cosmochimica Acta* 51: 2241–2253.

Barry TL, Pearce JA, Leat PT, Millar IL, and Le Roex AP (2006) Hf isotope evidence for selective mobility of high-field-strength elements in a subduction setting: South Sandwich Islands. *Earth and Planetary Science Letters* 252: 223–244.

Barth MG, McDonough WF, and Rudnick RL (2000) Tracking the budget of Nb and Ta in the continental crust. *Chemical Geology* 165: 197–213.

Bartolini A and Larson RL (2001) Pacific microplate and the Pangea supercontinent in the Early to Middle Jurassic. *Geology* 29: 735–738.

Bassett D, Sutherland R, Henrys S, et al. (2010) Three-dimensional velocity structure of the northern Hikurangi margin, Raukumara, New Zealand: Implications for the

growth of continental crust by subduction erosion and tectonic underplating. *Geochemistry, Geophysics, Geosystems* 11: Q10013.
Becker K, Sakai H, et al. (1988) Site 677 and 678. *Proceedings of the Ocean Drilling Program, Initial Reports (Part A)*, vol. 111, pp. 253–346. College Station, TX: Ocean Drilling Program.
Behrmann JH and Kopf A (2001) Balance of tectonically accreted and subducted sediment at the Chile Triple Junction. *International Journal of Earth Sciences* 90: 753–768.
Behrmann JH, Lewis SD, Musgrave RJ, et al. (1992) Site 863. *Proceedings of the Ocean Drilling Program, Initial Reports*, vol. 141, pp. 343–446. College Station, TX: Ocean Drilling Program.
Bouman C, Elliott T, and Vroon PZ (2004) Lithium inputs to subduction zones. *Chemical Geology* 212: 59–79.
Brenan JM, Neroda E, Lundstrom CC, Shaw HF, Ryerson FJ, and Phinney DL (1998a) Behaviour of boron, beryllium, and lithium during melting and crystallization constraints from mineral–melt partitioning experiments. *Geochimica et Cosmochimica Acta* 62: 2129–2141.
Brenan JM, Ryerson FJ, and Shaw HF (1998b) The role of aqueous fluids in the slab-to-mantle transfer of boron, beryllium, and lithium during subduction experiments and models. *Geochimica et Cosmochimica Acta* 62: 3337–3347.
Caciagli N, Brenan JM, McDonough WF, and Phinney D (2011) Mineral–fluid partitioning of lithium and implications for slab–mantle interaction. *Chemical Geology* 280: 384–398.
Carpentier M, Chauvel C, and Mattielli N (2008) Pb–Nd isotopic constraints on sedimentary input into the Lesser Antilles arc system. *Earth and Planetary Science Letters* 272: 199–211.
Carpentier M, Chauvel C, Maury RC, and Mattielli N (2009) The 'zircon effect' as recorded by the chemical and Hf isotopic compositions of Lesser Antilles forearc sediments. *Earth and Planetary Science Letters* 287: 86–99.
Carr MJ, Feigenson MD, and Bennet EA (1990) Incompatible element and isotopic evidence for tectonic control of source mixing and melt extraction along the Central American arc. *Contributions to Mineralogy and Petrology* 105: 369–380.
Carr MJ, Saginor I, Alvarado G, et al. (2007) Element fluxes from the volcanic front of Nicaragua and Costa Rica. *Geochemistry, Geophysics, Geosystems* 8: Q06001.
Carter RM, McCave IN, and Carter L (2004) Leg 181 synthesis: Fronts, flows, drifts, volcanoes, and the evolution of the southwestern gateway to the Pacific Ocean, eastern New Zealand. *Proceedings of Ocean Drilling Program, Scientific Results*, vol. 181, pp. 1–111. College Station, TX: Ocean Drilling Program.
Carter RM, McCave IN, Richter C, et al. (1999) Site 1124. *Proceedings of Ocean Drilling Program Initial Reports*, vol. 181, p. 137. College Station, TX: Ocean Drilling Program.
Castillo PR, Lonsdale PF, Moran CL, and Hawkins JW (2009) Geochemistry of mid-Cretaceous Pacific crust being subducted along the Tonga–Kermadec Trench: Implications for the generation of arc lavas. *Lithos* 112: 87–102.
Chan LH and Edmond JM (1988) Variation of lithium isotope composition in the marine environment: A preliminary report. *Geochimica et Cosmochimica Acta* 52: 1711–1717.
Chan LH, Edmond JM, Thompson G, and Gillis K (1992) Lithium isotope composition of submarine basalts – Implications for the lithium cycle in the oceans. *Earth and Planetary Science Letters* 108: 151–160.
Chan L-H, Leeman WP, and Plank T (2006) Lithium isotopic composition of marine sediments. *Geochemistry, Geophysics, Geosystems* 7: Q06005.
Chan LH, Leeman WP, and You CF (2002) Lithium isotopic composition of Central American volcanic arc lavas: Implications for modification of subarc mantle by slab-derived fluids: Correction. *Chemical Geology* 182: 293–300.
Chauvel C, Lewin E, Carpentier M, Arndt NT, and Marini J-C (2008) Role of recycled oceanic basalt and sediment in generating the Hf–Nd mantle array. *Nature Geoscience* 1: 64–67.
Chauvel C, Marini JC, Plank T, and Ludden JN (2009) Hf–Nd input flux in the Izu-Mariana subduction zone and recycling of subducted material in the mantle. *Geochemistry, Geophysics, Geosystems* 10: Q01001.
Chavagnac V, German CR, and Taylor RN (2008) Global environmental effects of large volcanic eruptions on ocean chemistry: Evidence from 'hydrothermal' sediments (ODP Leg 185, Site 1149B). *Journal of Geophysical Research* 113: B06201.
Class C, Miller DL, Goldstein SL, and Langmuir CH (2000) Distinguishing melt and fluid components in Umnak Volcanics, Aleutian Arc. *Geochemistry, Geophysics, Geosystems* 1(6): 1004.
Clift PD, Shimizu N, Layne GD, et al. (2001) Development of the Indus Fan and its significance for the erosional history of the Western Himalaya and Karakoram. *Geological Society of America Bulletin* 13: 1039–1051.
Condie KC (1993) Chemical composition and evolution of the upper continental crust: Contrasting results from surface samples and shales. *Chemical Geology* 104: 1–37.
Contreras-Reyes E, Flueh ER, and Grevemeyer I (2010) Tectonic control on sediment accretion and subduction off south central Chile: Implications for coseismic rupture processes of the 1960 and 2010 megathrust earthquakes. *Tectonics* 29: 27.
Cooper L (2009) *Volatiles in Tonga Arc Magmas and Their Role in Unraveling Subduction Zone Processes*. PhD Thesis, Boston University.
Cousens BL, Allan JF, and Gorton MP (1994) Subduction-modified pelagic sediments as the enriched component in back-arc basalts from the Japan Sea: Ocean Drilling Program Sites 797 and 794. *Contributions to Mineralogy and Petrology* 117: 421–434.
Davy B, Hoernle K, and Werner R (2008) Hikurangi Plateau: Crustal structure, rifted formation, and Gondwana subduction history. *Geochemistry, Geophysics, Geosystems* 9: Q07004.
Dohmen R, Kasemann SA, Coogan L, and Chakraborty S (2010) Diffusion of Li in olivine. Part I: Experimental observations and a multi species diffusion model. *Geochimica et Cosmochimica Acta* 74: 274–292.
Elliott T, Plank T, Zindler A, White W, and Bourdon B (1997) Element transport from subducted slab to volcanic front at the Mariana arc. *Journal of Geophysical Research* 102: 14991–15019.
Galy A, France-Lanord C, and Derry LA (1996) The Late Oligocene-Early Miocene Himalayan belt Constraints deduced from isotopic compositions of Early Miocene turbidites in the Bengal Fan. *Tectonophysics* 260: 109–118.
Gamble J, Woodhead J, Wright I, and Smith I (1996) Basalt and sediment geochemistry and magma petrogenesis in a transect from oceanic island arc to rifted continental margin arc: The Kermadec–Hikurangi margin, SW Pacific. *Journal of Petrology* 37: 1523–1546.
Gao S, Luo T-C, Zhang B-R, et al. (1998) Chemical composition of the continental crust as revealed by studies in east China. *Geochimica et Cosmochimica Acta* 62: 1959–1975.
Goldstein SJ and Jacobsen SB (1987) Nd and Sr isotopic systematics of river water suspended material: Implications for crustal evolution. *Earth and Planetary Science Letters* 87: 249–265.
Goldstein SL, O'Nions RK, and Hamilton PJ (1984) A Sm–Nd isotopic study of atmospheric dusts and particulates from major river systems. *Earth and Planetary Science Letters* 70: 221–236.
Grove TL, Parman SW, Bowring SA, Price RC, and Baker MB (2002) The role of an $H_2O$-rich fluid component in the generation of primitive basaltic andesites and andesites from the Mt. Shasta region, N. California. *Contributions to Mineralogy and Petrology* 142: 375–396.
Halama R, Savov IP, Rudnick RL, and McDonough WF (2009) Insights into Li and Li isotope cycling and sub-arc metasomatism from veined mantle xenoliths, Kamchatka. *Contributions to Mineralogy and Petrology* 158: 197–222.
Handwerger DA and Jarrard RD (2003) Neogene changes in Southern Ocean sedimentation based on mass accumulation rates at four continental margins. *Paleoceanography* 18: 1081.
Hawkesworth CJ, Gallagher K, Hergt JM, and McDermott F (1993) Mantle and slab contributions in arc magmas. *Annual Review of Earth and Planetary Sciences* 21: 175–204.
Heath GR, Kovar RB, and Lopez C (1985) Geochemistry of sediments at Sites 579, 580, and 581, Deep Sea Drilling Project Leg 86, Western North Pacific. In: Heath GR and Burckle LH, et al. (eds.) *Initial Reports of the Deep Sea Drilling Project*, vol. 86, pp. 657–670. Washington, DC: US Government Printing Office.
Heberer B, Roser G, Behrmann JH, Rahn M, and Kopf A (2010) Holocene sediments from the Southern Chile Trench: A record of active margin magmatism, tectonics and palaeoseismicity. *Journal of the Geological Society* 167: 539–553.
Hein JR, Sancetta C, and Morgenson LA (1983) Petrology and geochemistry of silicified upper Miocene chalk, Costa Rica Rift, Deep Sea Drilling Project Leg 69. In: Cann JR, Langseth MG, and Honnorez J, et al. (eds.) *Initial Reports of the Deep Sea Drilling Project*, vol. 69, pp. 395–409. Washington, DC: US Government Printing Office.
Hermann J and Rubatto D (2009) Accessory phase control on the trace element signature of sediment melts in subduction zones. *Chemical Geology* 265: 512–526.
Hermann J and Spandler CJ (2008) Sediment melts at sub-arc depths: An experimental study. *Journal of Petrology* 49: 717–740.
Hoernle K, Hauff F, van den Bogaard P, et al. (2010) Age and geochemistry of volcanic rocks from the Hikurangi and Manihiki oceanic Plateaus. *Geochimica et Cosmochimica Acta* 74: 7196–7219.
Hofmann AW, Jochum KP, Seufert M, and White WM (1986) Nb and Pb in oceanic basalts: New constraints on mantle evolution. *Earth and Planetary Science Letters* 79: 33–45.
Hole MJ, Saunders AD, Marriner GF, and Tarney J (1984) Subduction of pelagic sediments: Implications for the origin of Ce-anomalous basalts from the Mariana Islands. *Journal of the Geological Society* 141: 453–472.
Ishikawa T and Nakamura E (1993) Boron isotope systematics of marine sediments. *Earth and Planetary Science Letters* 117: 567–580.

Jenkyns H (1976) Sediments and sedimentary history of the Manihiki Plateau, South Pacific Ocean. In: Schlanger SO, Jackson ED, Kaneps A, and Serocki ST (eds.) *Initial Reports of the Deep Sea Drilling Project*, vol. 33, pp. 873–890. Washington, DC: US Government Printing Office.

Jicha BR, Singer BS, Brophy JG, et al. (2004) Variable impact of the subducted slab on Aleutian island arc magma sources: Evidence from Sr, Nd, Pb, and Hf isotopes and trace element abundances. *Journal of Petrology* 45: 1845–1875.

Jochum KP, Stolz AJ, and McOrist G (2000) Niobium and tantalum in carbonaceous chondrites: Constraints on the solar system and primitive mantle niobium/tantalum, zirconium/niobium, and niobium/uranium ratios. *Meteoritics and Planetary Science* 35: 229–235.

Johnson MC and Plank T (1999) Dehydration and melting experiments constrain the fate of subducted sediments. *Geochemistry, Geophysics, Geosystems* 1: 1007.

Kamber BS, Greig A, and Collerson KD (2005) A new estimate for the composition of weathered young upper continental crust from alluvial sediments, Queensland, Australia. *Geochimica et Cosmochimica Acta* 69: 1041–1058.

Kamber BS, Greig A, Schoenberg R, and Collerson KD (2003) A refined solution to Earth's hidden niobium: Implications for evolution of continental crust and mode of core formation. *Precambrian Research* 126: 289–308.

Karl SM, Wandless GA, and Karpoff AM (1992) Sedimentological and geochemical characteristics of ODP Leg 129 siliceous deposits. In: Larson R, Lancelot Y, et al. (eds.) *Proceedings of Ocean Drilling Program, Scientific Results*, vol. 129, pp. 31–80. College Station, TX: Ocean Drilling Program.

Kelley KA, Plank T, Ludden JN, and Staudigel H (2003) The composition of altered oceanic crust at ODP sites 801 and 1149. *Geochemistry, Geophysics, Geosystems* 4(6): 8910.

Kersting AB (1995) Pb isotope ratios of North Pacific sediments, Sites 881, 883, and 884: Implications for sediment recycling in the Kamchatkan arc. In: Rea DK, Basov IA, Scholl DW, and Allan JF (eds.) *Proceedings of the Ocean Drilling Program, Scientific Results*, vol. 145, pp. 383–388. College Station, TX: Ocean Drilling Program.

Kessel R, Schmidt MW, Ulmer P, and Pettke T (2005) Trace element signature of subduction-zone fluids, melts and supercritical liquids at 120–180 km depth. *Nature* 437: 724–727.

Kilian R and Behrmann JH (2003) Geochemical constraints on the sources of Southern Chile trench sediments and their recycling in arc magmas of the Southern Andes. *Journal of the Geological Society* 160: 57–70.

Klimm K, Blundy JD, and Green TH (2008) Trace element partitioning and accessory phase saturation during $H_2O$-saturated melting of basalt with implications for subduction zone chemical fluxes. *Journal of Petrology* 49: 523–553.

Koppers AAP, Staudigel H, and Duncan AR (2003) High-resolution $^{40}Ar/^{39}Ar$ dating of the oldest oceanic basement basalts in the western Pacific Basin. *Geochemistry, Geophysics, Geosystems* 4: 8914.

Koschinsky A and Hein JR (2003) Uptake of elements from seawater by ferromanganese crusts: Solid-phase associations and seawater speciation. *Marine Geology* 198: 331–351.

LaGatta AB (2002) *Arc Magma Genesis in the Eastern Mexican Volcanic Belt*. PhD Thesis, Columbia University.

Leat PT, Pearce JA, Barker PF, Millar IL, Barry TL, and Larter RD (2004) Magma genesis and mantle flow at a subducting slab edge: The South Sandwich arc-basin system. *Earth and Planetary Science Letters* 227: 17–35.

Leeman WP (1996) Boron and other fluid-mobile elements in volcanic arc lavas: Implications for subduction processes. In: Bebout GE, Scholl W, Kirby H, and Platt P (eds.) *Subduction: Top to Bottom*. *Geophysical Monograph Series*, vol. 96, pp. 269–276. Washington, DC: American Geophysical Union.

Leeman WP, Tonarini S, Chan LH, and Borg LE (2004) Boron and lithium isotopic variations in a hot subduction zone – The southern Washington Cascades. *Chemical Geology* 212: 101–124.

Leggett JM (1982) Geochemistry of Cocos Plate pelagic–hemipelagics ediments in Hole 487, Deep Sea Drilling Project Leg 66. In: Watkins JS, Moore JC, et al. (eds.) *Initial Reports of the Deep Sea Drilling Project*, vol. 66, pp. 683–686. Washington, DC: US Government Printing Office.

Li Y-H and Schoonmaker JE (2003) Chemical composition and mineralogy of marine sediments. In: Mackenzie FT (ed.) *Treatise on Geochemistry, Sediments, Diagenesis and Sedimentary Rocks*, Vol. 7, pp. 1–35. Oxford: Elsevier-Pergamon.

Lucassen F, Wiedicke M, and Franz ZG (2010) Complete recycling of a magmatic arc: Evidence from chemical and isotopic composition of Quaternary trench sediments in Chile (36°–40°S). *International Journal of Earth Sciences* 99: 687–701.

Magna T, Wiechert U, Grove TL, and Halliday AN (2006) Lithium isotope fractionation in the southern Cascadia subduction zone. *Earth and Planetary Science Letters* 250: 428–443.

Marschall HR, Altherr R, and Rüpke L (2007a) Squeezing out the slab – Modelling the release of Li, Be and B during progressive high-pressure metamorphism. *Chemical Geology* 239: 323–335.

Marschall HR, Pogge von Strandmann PAE, Seitz HM, Elliott T, and Niu Y (2007b) The lithium isotopic composition of orogenic eclogites and deep subducted slabs. *Earth and Planetary Science Letters* 262: 563–580.

Marx SK and Kamber BS (2010) Trace-element systematics of sediments in the Murray–Darling Basin, Australia: Sediment provenance and palaeoclimate implications of fine scale chemical heterogeneity. *Applied Geochemistry* 25: 1221–1237.

McDonough WF (1991) Partial melting of subducted oceanic crust and isolation of its residual eclogitic lithology. *Philosophical Transactions of the Royal Society Series A* 335: 407–418.

McDonough WF and Sun SS (1995) The composition of the Earth. *Chemical Geology* 120: 223–253.

McLennan SM, Taylor SR, McCulloch MT, and Maynard JB (1990) Geochemical and Nd–Sr isotopic composition of deep-sea turbidites: Crustal evolution and plate tectonic associations. *Geochimica et Cosmochimica Acta* 54: 2015–2050.

Miller DM, Goldstein SL, and Langmuir CH (1994) Cerium–lead and lead-isotope ratios in arc magmas and the enrichment of lead in the continents. *Nature* 368: 514–520.

Mix AC, Tiedemann R, Blum P, et al. (2003) Site 1232. *Proceedings of the Ocean Drilling Program, Initial Reports*, vol. 202, pp. 1–54. College Station, TX: Ocean Drilling Program.

Moriguti T and Nakamura E (1998) Across-arc variation of Li isotopes in lavas and implications for crust/mantle recycling at subduction zones. *Earth and Planetary Science Letters* 163: 167–174.

Morris JD, Leeman WP, and Tera F (1990) The subducted component in island arc lavas: Constraints form Be isotopes and B–Be systematics. *Nature* 344: 31–36.

Morris JD, Villinger HW, Klaus A, et al. (2003) *Proceedings of the Ocean Drilling Program, Initial Reports*, vol. 205. College Station, TX: Ocean Drilling Program.

Mueller PA, Shuster RD, Darcy KA, Heatherington AL, Nutman AP, and Williams IS (1995) Source of the northeastern Idaho Batholith – Isotopic evidence for a paleoproterozoic terrane in the northwestern US. *Journal of Geology* 103: 63–72.

Munker C, Pfander JA, Weyer S, Buchl A, Kleine T, and Mezger K (2003) Evolution of planetary cores and the Earth–Moon system from Nb/Ta systematics. *Science* 301: 84–87.

Nebel O, van Westrenen W, Vroon PZ, Wille M, and Raith MM (2010) Deep mantle storage of the Earth's missing niobium in late-stage residual melts from a magma ocean. *Geochimica et Cosmochimica Acta* 74: 4392–4404.

Niu Y and Batiza R (1997) Trace element evidence from seamounts for recycled oceanic crust in the eastern Pacific mantle. *Earth and Planetary Science Letters* 148: 471–483.

Noll PD, Newsom HE, Leeman WP, and Ryan JG (1996) The role of hydrothermal fluids in the production of subduction zone magmas: Evidence from siderophile and chalcophile trace elements and boron. *Geochimica et Cosmochimica Acta* 60: 587–611.

Patino LC, Carr MJ, and Feigenson MD (2000) Local and regional variations in Central American arc lavas controlled by variations in subducted sediment input. *Contributions to Mineralogy and Petrology* 138: 265–283.

Pearce JA, Baker PE, Harvey PE, and Luff IW (1995) Geochemical evidence for subduction fluxes, mantle melting and fractional crystallization beneath the South Sandwich Island Arc. *Journal of Petrology* 36: 1073–1109.

Pearce JA, Kempton PD, and Gill JB (2007) Hf–Nd evidence for the origin and distribution of mantle domains in the SW Pacific. *Earth and Planetary Science Letters* 260: 98–114.

Pearce JA, Kempton PD, Nowell GM, and Noble SR (1999) Hf–Nd element and isotope perspective on the nature and provenance of mantle and subduction components in western Pacific arc-basin systems. *Journal of Petrology* 40: 1579–1611.

Pearce JA, Stern RJ, Bloomer SH, and Fryer P (2005) Geochemical mapping of the Mariana arc-basin system: Implications for the nature and distribution of subduction components. *Geochemistry, Geophysics, Geosystems* 6: Q07006.

Peate DW, Pearce JA, Hawkesworth CJ, Colley H, Edwards CMH, and Hirose K (1997) Geochemical variations in Vanuatu arc lavas: The role of subducted material and a variable mantle wedge composition. *Journal of Petrology* 38: 1331–1358.

Peucker-Ehrenbrink B, Miller MW, Arsouze T, and Jeandel C (2010) Continental bedrock and riverine fluxes of strontium and neodymium isotopes to the oceans. *Geochemistry, Geophysics, Geosystems* 11: Q03016.

Plank T (2005) Constraints from thorium/lanthanum on sediment recycling at subduction zones and the evolution of continents. *Journal of Petrology* 46: 921–944.

Plank T, Balzer V, and Carr MJ (2002) Nicaraguan volcanoes record paleoceanographic changes accompanying closure of the Panama gateway. *Geology* 30: 1087–1090.

Plank T, Cooper L, and Manning CE (2009) New geothermometers for estimating slab surface temperatures. *Nature Geoscience* 2: 611–615.

Plank T, Kelley KA, Murray RW, and Stern LQ (2007) Chemical composition of sediments subducting at the Izu-Bonin trench. *Geochemistry, Geophysics, Geosystems* 8: Q04I16.

Plank T and Langmuir CH (1993) Tracing trace element from sediment input to volcanic output at subduction zones. *Nature* 362: 739–742.

Plank T and Langmuir CH (1998) The chemical composition of subducting sediment and its consequences for the crust and mantle. *Chemical Geology* 145: 325–394.

Plank T and Ludden JN (1992) Geochemistry of sediments in the Argo Abyssal plain at ODP Site 765: A continental margin reference section for sediment recycling in subduction zones. In: Gradstein FM and Ludden JN, et al. (eds.) *Proceedings of the Ocean Drilling Program, Scientific Results*, vol. 123, pp. 167–189. College Station, TX: Ocean Drilling Program.

Plank T, Ludden J, Escutia C, et al. (2000) Leg 185. *Proceedings of the Ocean Drilling Program, Initial Reports*, vol. 185. College Station, TX: Ocean Drilling Program.

Prueher LM and McBirney AR (1988) Relations of cinder cones to the magmatic evolution of Mount Mazama, Crater Lake National Park, Oregon. *Journal of Volcanology and Geothermal Research* 35: 253–268.

Prytulak J, Vervoort JD, Plank T, and Yu C (2006) Astoria fan sediments, DSDP Site 174, Cascadia Basin: Hf–Nd–Pb constraints on provenance and outburst flooding. *Chemical Geology* 233: 276–292.

Qiu L, Rudnick RL, Ague JJ, and McDonough WF (2011) A lithium isotopic study of sub-greenschist to greenschist facies metamorphism in an accretionary prism, New Zealand. *Earth and Planetary Science Letters* 301: 213–221.

Qiu L, Rudnick RL, McDonough WF, and Merriman RJ (2009) Li and $\delta^7$Li in mudrocks from the British Caledonides: Metamorphism and source influences. *Geochimica et Cosmochimica Acta* 73: 7325–7340.

Rodriguez C, Selles D, Dungan M, Langmuir C, and Leeman W (2007) Adakitic dacites formed by intracrustal crystal fractionation of water-rich parent magmas at Nevado de Longavi Volcano (36.2°S; Andean Southern Volcanic Zone, Central Chile). *Journal of Petrology* 48: 2033–2061.

Rudnick RL, Barth M, Horn I, and McDonough WF (2000) Rutile-bearing refractory eclogites: Missing link between continents and depleted mantle. *Science* 287: 278–281.

Ryan JG and Langmuir CH (1987) The systematics of lithium abundances in young volcanic rocks. *Geochimica et Cosmochimica Acta* 51(6): 1727–1741.

Sageman BB and Lyons TW (2003) Geochemistry of fine-grained sediments and sedimentary rocks. In: Mackenzie FT (ed.) *Treatise on Geochemistry, Sediments, Diagenesis and Sedimentary Rocks*, vol. 7, pp. 115–158. Oxford: Elsevier-Pergamon.

Schmidt MW, Dardon A, Chazot G, and Vannucci R (2004a) The dependence of Nb and Ta rutile-melt partitioning on melt composition and Nb/Ta fractionation during subduction processes. *Earth and Planetary Science Letters* 226: 415–432.

Schmidt MW, Vielzeuf D, and Auzanneau E (2004b) Melting and dissolution of subducting crust at high pressures: The key role of white mica. *Earth and Planetary Science Letters* 228: 65–84.

Scudder R, Murray RW, and Plank T (2009) Dispersed ash in deeply buried sediment from the northwest Pacific Ocean: An example from the Izu-Bonin arc (ODP Site 1149). *Earth and Planetary Science Letters* 284: 639–648.

Singer BS, Jicha BR, Leeman WP, et al. (2007) Along-strike trace element and isotopic variation in Aleutian Island arc basalt: Subduction melts sediments and dehydrates serpentine. *Journal of Geophysical Research* 112: B06206.

Skora S and Blundy J (2010) High-pressure hydrous phase relations of radiolarian clay and implications for the involvement of subducted sediment in arc magmatism. *Journal of Petrology* 51: 2211–2243.

Staudigel H, Plank T, White WM, and Schmincke H (1996) Geochemical fluxes during seafloor alteration of the upper oceanic crust: DSDP Sites 417 and 418. In: Bebout GE, Scholl W, Kirby H, and Platt P (eds.) *Subduction: Top to Bottom. Geophysical Monograph Series*, vol. 96, pp. 19–38. Washington, DC: American Geophysical Union.

Summerhayes CP and Gilbert D (1982) Distribution, origin and hydrocarbon potential of organic matter in sediments from the Pacific margin of Guatemala. In: Aubouin J, von Huene R, et al. (eds.) *Initial Reports of the Deep Sea Drilling Project*, vol. 67, pp. 595–599. Washington, DC: US Government Printing Office.

Syracuse EM and Abers GA (2006) Global compilation of variations in slab depth beneath arc volcanoes and implications. *Geochemistry, Geophysics, Geosystems* 7: Q05017.

Takahashi Y, Manceau A, Geoffroy N, Marcus MA, and Usui A (2007) Chemical and structural control of the partitioning of Co, Ce, and Pb in marine ferromanganese oxides. *Geochimica et Cosmochimica Acta* 71: 984–1008.

Tatsumi Y, Murasaki M, Arsadi EM, and Nohda S (1991) Geochemistry of Quaternary lavas from NE Sulawesi: Transfer of subduction components into the mantle wedge. *Contributions to Mineralogy and Petrology* 107: 137–149.

Taylor SR and McLennan SM (1985) *The Continental Crust: Its Composition and Evolution*. Oxford: Blackwell.

Teng F-Z, McDonough WF, Rudnick RL, and Wing BA (2007) Limited lithium isotopic fractionation during progressive metamorphic dehydration in metapelites: A case study from the Onawa contact aureole, Maine. *Chemical Geology* 239: 1–12.

Teng F-Z, McDonough WF, Rudnick RL, et al. (2004) Lithium isotopic composition and concentration of the upper continental crust. *Geochimica et Cosmochimica Acta* 68: 4167–4178.

Tera F, Brown L, Morris J, Sacks IS, Klein J, and Middleton R (1986) Sediment incorporation in island-arc magmas: Inferences from 10 Be. *Geochimica et Cosmochimica Acta* 50: 535–550.

Todd E, Gill JB, Wysoczanski RJ, Handler MR, Wright IC, and Gamble JA (2010) Sources of constructional cross-chain volcanism in the southern Havre Trough: New insights from HFSE and REE concentration and isotope systematics. *Geochemistry, Geophysics, Geosystems* 11: Q04009.

Tollstrup D, Gill J, Kent A, et al. (2010) Across-arc geochemical trends in the Izu-Bonin arc: Contributions from the subducting slab, revisited. *Geochemistry, Geophysics, Geosystems* 11: Q01X10.

Tomascak PB (2004) Developments in the understanding and application of lithium isotopes in the earth and planetary sciences. In: Johnson CM, Beard BL, and Albarede F (eds.) *Geochemistry of Non-Traditional Stable Isotopes. Reviews in Mineralogy*, vol. 55, pp. 153–195. Washington, DC: Mineralogical Society of America.

Tomascak PB, Widom E, Benton LD, Goldstein SL, and Ryan JG (2002) The control of lithium budgets in island arcs. *Earth and Planetary Science Letters* 196: 227–238.

Tonarini S, Leeman WP, and Leat PT (2011) Subduction erosion of forearc mantle wedge implicated in the genesis of the South Sandwich Island (SSI) arc: Evidence from boron isotope systematics. *Earth and Planetary Science Letters* 301: 275–284.

Trotter JA and Eggins SM (2006) Chemical systematics of conodont apatite determined by laser ablation ICPMS. *Chemical Geology* 233: 196–216.

Turner ST, Hawkesworth C, van Calsteren P, Heath E, Macdonald R, and Black S (1996) U-series isotopes and destructive margin magma genesis in the Lesser Antilles. *Earth and Planetary Science Letters* 142: 191–207.

van de Flierdt T, Frank M, Halliday AN, et al. (2003) Lead isotopes in North Pacific deep water – Implications for past changes in input sources and circulation patterns. *Earth and Planetary Science Letters* 209: 149–164.

Veizer J and Mackenzie FT (2003) Evolution of sedimentary rocks. In: Mackenzie FT (ed.) *Treatise on Geochemistry, Sediments, Diagenesis and Sedimentary Rocks*, Vol. 7, pp. 369–407. Oxford: Elsevier-Pergamon.

Vengosh A, Kolodny Y, Starinsky A, Chivas AR, and McCulloch MT (1991) Coprecipitation and isotopic fractionation of boron in modern biogenic carbonates. *Geochimica et Cosmochimica Acta* 55: 2901–2910.

Vervoort J, Prytulak J, and Plank T (2011) The Hf–Nd isotopic composition of marine sediments. *Geochimica et Cosmochimica Acta* 75(20): 5903–5926.

Vils F, Tonarini S, Kalt A, and Seitz H-M (2009) Boron, lithium and strontium isotopes as tracers of seawater–serpentinite interaction at Mid-Atlantic ridge, ODP Leg 209. *Earth and Planetary Science Letters* 286: 414–425.

Vlastelic I, Abouchami W, Galer SJG, and Hofmann A (2001) Geographic control on Pb isotope distribution and sources in Indian Ocean Fe–Mn deposits. *Geochimica et Cosmochimica Acta* 65: 4303–4319.

von Drach V, Marsh BD, and Wasserburg GJ (1986) Nd and Sr isotopes in the Aleutians: Multicomponent parenthood of island arc magmas. *Contributions to Mineralogy and Petrology* 92: 13–34.

von Huene R and Scholl DW (1991) Observations at convergent margins concerning sediment subduction, subduction erosion, and the growth of continental crust. *Reviews of Geophysics* 29: 279.

Wade J and Wood BJ (2001) The Earth's 'missing' niobium may be in the core. *Nature* 409: 75–78.

Weedon GP and Hall IR (2002) Data report: Inorganic geochemistry of Miocene to recent samples from Chatham Rise, Southwest Pacific, Site 1123. In: Richter C (ed.) *Proceedings of the Ocean Drilling Program, Scientific Results*, vol. 181, pp. 1–10. College Station, TX: Ocean Drilling Program.

Woodhead JD (1989) Geochemistry of the Mariana arc western Pacific: Source composition and processes. *Chemical Geology* 76: 1–24.

Woodhead JD, Hergt JM, Davidson JP, and Eggins SM (2001) Hafnium isotope evidence for 'conservative' element mobility during subduction zone processes. *Earth and Planetary Science Letters* 192: 331–346.

Wunder B, Meixner A, Romer RL, and Heinrich W (2006) Temperature-dependent isotopic fractionation of lithium between clinopyroxene and high-pressure fluids. *Contributions to Mineralogy and Petrology* 151: 112–120.

You CF, Chan LH, Spivak AJ, and Gieskes JM (1995) Lithium, boron, and their isotopes in sediments and pore waters of ODP Site 808, Nankai Trough: Implications for fluid expulsion in accretionary prisms. *Geology* 23: 37–40.

Zack T, Tomascak PB, Rudnick RL, Dalpe C, and McDonough WF (2003) Extremely light Li in orogenic eclogites: The role of isotope fractionation during dehydration in subducted oceanic crust. *Earth and Planetary Science Letters* 208: 279–290.

Zhou L (1990) *Characterization of Chemical Signatures in Sediments: Applications to Selected Problems*. PhD Thesis, University of California, Los Angeles.

Zhou L and Kyte FT (1992) Sedimentation history of the South Pacific pelagic clay province over the last 85 million years inferred from the geochemistry of DSDP Hole 596. *Paleoceanography* 7: 441–465.